A Broad Anti-influenza Hybrid Small Molecule That Potently Disrupts the Interaction of Polymerase Acidic Protein−Basic Protein 1 (PA-PB1) Subunits

Serena Massari,[§,⊥] Giulio Nannetti,[¥,⊥] Jenny Desantis,[§] Giulia Muratore,[¥] Stefano Sabatini,[§] Giuseppe Manfroni,[§] Beatrice Mercorelli,[¥] Violetta Cecchetti,[§] Giorgio Palù,[¥] Gabriele Cruciani,[#] Arianna Loregian,[¥,*,⊥] Laura Goracci,[#,*] and Oriana Tabarrini.[§,*,⊥]

Department of Pharmaceutical Sciences, University of Perugia, 06123 Perugia, Italy, Department of Molecular Medicine, University of Padua, 35121 Padua, Italy, Department of Chemistry, Biology and Biotechnology, University of Perugia, 06123 Perugia, Italy.

TITLE RUNNING HEAD: Polymerase PA-PB1 interaction triazolopyrimidine inhibitors with anti-influenza activity.

[*] To whom correspondence should be addressed. For OT: phone, + 39 075 585 5139; fax, +39 075 585 5115; e-mail, oriana.tabarrini@unipg.it. For AL: phone, +39 049 8272363; fax, +39 049 8272355; e-mail, arianna.loregian@unipd.it. For LG: phone, +39 075 585 5632; fax, +39 075 45646; e-mail, laura.goracci@unipg.it.

[⊥] Authors contributed equally to this work.

[§] Department of Pharmaceutical Sciences.

[¥] Department of Molecular Medicine.

[#] Department of Chemistry, Biology, and Biotechnology.

ABSTRACT

In continuing our efforts to identify small molecules able to disrupt PA-PB1 subunits interaction of influenza virus (Flu) RNA-dependent RNA polymerase, this paper was devoted to the optimization of a dihydrotriazolopyrimidine derivative, previously identified through a structure-based drug discovery. The structure modifications performed around the bicyclic core led to the identification of compounds endowed with both the ability to disrupt PA-PB1 subunits interaction and anti-Flu activity with no cytotoxicity. Very interesting results were obtained with the hybrid molecules **36** and **37**, designed by merging some peculiar structural features known to impart PA-PB1 interaction inhibition, with compound **36** that emerged as the most potent PA-PB1 interaction inhibitor (IC_{50} of 1.1 μM) among all the small molecules reported so far. Calculations showed a very favored H-bonding between the 2-amidic carbonyl of **36** and Q408, which seems to justify its potent ability to interfere with the polymerase subunits interaction.

INTRODUCTION

Influenza is a highly contagious, acute, febrile, respiratory illness. Only two classes of drugs are currently available to treat influenza infections, i.e., M2 ion channel inhibitors and neuraminidase inhibitors. Unfortunately, their clinical use is limited by serious side effects, low efficacy, and the emergence of resistant virus variants.[1–3] Because of these issues, the M2 ion channel inhibitors are no longer even recommended;[4] thus, the neuraminidase inhibitors, such as oseltamivir, represent the firstline therapy, although their widespread use has been reported to favor the emergence of resistant viral strains.[5] Clearly, new anti-influenza virus (Flu) strategies based on alternative mechanisms of action are strongly needed. Along this line, we have chosen the viral RNA-dependent RNA polymerase (RdRP) as a valid antiviral target since it is essential for virus replication and plays an important role in the viral pathogenesis by contributing to the host-adaptation process. In addition, it is highly conserved among FluA, -B, and -C, and its mechanism of action significantly differs from that of the human RNA polymerases.[6] Flu RdRP is a complex of

three subunits, polymerase acidic protein (PA), polymerase basic protein 1 (PB1), and polymerase basic protein 2 (PB2), whose correct assembly into functional RdRP is an essential step for Flu RNA synthesis and replication. The inhibition of protein−protein interactions (PPIs) between the subunits of the viral RNA polymerase represents an attractive as well as challenging strategy that could expand the narrow target spectrum of anti-Flu drugs.[7−9] Previous studies have revealed that the N-terminal and the C-terminal regions of PB1 interact with the C-terminus of PA [10−14] and the N-terminus of PB2, [11,15] respectively. While no small molecule targeting the PB1−PB2 interaction is known, with only a few short peptides reported for this activity, [16,17] various small molecules that are able to disrupt the interactions between the PA and PB1 subunits have emerged during the past 3 years.[18−25] Their PPI inhibitory activity correlated to the inhibition of viral RdRP activity and of virus replication in a cellular context, thus validating this antiviral strategy. Different approaches led to identification of the PA−PB1 small molecule inhibitors reported so far (Figure 1). Nitrobenzofurazan derivatives have emerged from a biochemical ELISA-based screening,[21] which was followed by an optimization study that gave compound 123 as one of the most active. drug discovery (SBDD) strategy. In particular, compounds **3** (benzbromarone)[19] and **4** (diclazuril)[19] came from an in silico screening performed on a database of 4000 drugs, while by screening 3 million small molecules we have discovered the promising hit compounds **5−8**.[18] A successive round of optimization performed on compounds **6** and **7** led to the improved derivatives **9** [22] and **10** [22] (Figure 1), whose anti-Flu activity also encompassed a panel of clinical isolates of FluA, including an oseltamivir-resistant strain, and of FluB, without showing appreciable cytotoxicity. In this study, with the aim of broadening the class of PA−PB1 interaction inhibitors as alternative anti-Flu agents, the optimization of the dihydrotriazolopyrimidine derivative 8 is reported. On the other hand, anthracene derivative **220** was discovered by serendipity. However, the largest number of PA−PB1 interaction inhibitors was identified through a structure-based.

DESIGN OF TRIAZOLOPYRIMIDINE DERIVATIVES

Among the hit compounds previously identified, the dihydrotriazolopyrimidine derivative **8** showed a weak PA-PB1 interaction inhibitory activity (IC_{50} = 170.6 μM) and no antiviral activity up to 100 μM, but the lack of any cytotoxic effect (CC_{50} > 250 μM in MDCK cells)[9] made it worthy of further investigation. The structural modifications were initially focused on the benzamide moiety at the C-2 position (Table 1). The methoxy group was run into *ortho* and *meta* positions (compounds **11** and **12**) and an analogous set of derivatives was synthesized having a fluorine atom (compounds **13**-**15**). Since in these two series of compounds the *para* derivatives were slightly more active than the other isomers, the successive substituents were placed only at the *para* position, synthesizing compounds **16-24**. Additional derivatives were **25**, characterized by a bicyclic aromatic ring, **26**, devoid of any substituent on the phenyl ring, and **27**, where an ethyl chain was inserted between the phenyl ring and the amide moiety. Since some difficulties were encountered with the purification of this first series of derivatives, the 4,7-dihydro-[1,2,4]triazolo[1,5-a]pyrimidine nucleus was oxidized leading to more manageable aromatic compounds. Derivatives **28-30** were synthesized using the phenyl, the *p*-methoxyphenyl, and *p*-propoxyphenyl rings, respectively, as C-2 substituents.

Previous computational studies indicated that a more linear shape of the compounds could increase the inhibitory effect.[15] Moreover, the alignment of the 1,2,4-triazolo[1,5-a]pyrimidine derivative **28** to the recently published pharmacophore for PA-PB1 inhibitors[15] (Figure 2, A and B), indicated that the 7-phenyl ring was not fitting any hydrophobic pharmacophoric point (green spheres in Figure 2) but, on the contrary, it was pointing towards polar atomic coordinates (red and blue spheres in Figure 2). In the light of the above considerations, we decided to further modify the central core by interchanging the methyl and the phenyl ring, synthesizing compounds **31-33**. Figure 2C reports the alignment of **31** to the pharmacophore.

Since the H-bond acceptor and H-bond donor pharmacophoric points underneath the amide group proved to be essential for pharmacophore definition,[15] the presence of an inverse amide group linking the triazolopyrimidine core and the phenyl ring was studied by synthesizing the couple of positional isomers **34** and **35**.

Finally, as additional analogues of **8**, hybrid molecules were designed by combining some of the structural features shown to confer PA-PB1 inhibitory activity.[9,13,15] Among the planned molecules, the positional isomers **36** and **37** (Table 1) were synthesized by merging the 1,2,4-triazolopyrimidine nucleus with the cycloheptathiophene-3-carboxamide core that characterizes the previous hit **7** (Figure 1). The two hybrid molecules were aligned to the pharmacophore, obtaining a good similarity both for polar and hydrophobic regions (Figure 3), with the 1,2,4-triazolopyrimidine nucleus being oriented in the lower hydrophobic region of the pharmacophore, in an opposite way to compounds **28** and **31** (Figure 2), to gain the better alignment of the polar regions.

CHEMISTRY

The synthesis of all the target compounds was accomplished through a carbodiimide-mediated coupling reaction by reacting the 2-amino and 2-carboxylic acid 1,2,4-triazolo[1,5-a]pyrimidine synthones with the appropriate benzoyl chlorides and amines, respectively. Although the triazolopyrimidines chemistry has been widely explored,[26] very few reports were focused on the synthesis of 2-amino and 2-carboxylic acid 1,2,4-triazolo[1,5-a]-pyrimidine derivatives. Thus, the synthesis of the synthones **38**, **41**, **42**, **45**, and **47** required an in-depth study aimed to determine the best synthetic pathway and conditions to obtain the desired positional isomers in high yield. In Schemes 1 and 2, selected procedures among those reported in the literature or appositely setup are shown, while a thorough comparative study will be reported in due course. Synthone **38** [27] was prepared as reported in the literature, by reacting 3,5-diamino-1,2,4-triazole with benzylideneacetone in DMF at reflux (Scheme 1). The same reaction was applied to prepare synthone **41** [28] (Scheme 1), but adding Ac_2O to the reaction mixture after the condensation completion, in order to protect the amino group in the successive oxidation step. The oxidation of compound **39** performed with N-bromosuccinimide (NBS) gave intermediate 40, which after acid hydrolysis gave the desired synthone **41**. An analogous three-step procedure was planned to synthesize the unknown synthone **42** by reacting 3,5-diamino-1,2,4-triazole with phenyl 1-propenyl

ketone in DMF at reflux (Scheme 1). Fortunately, the reaction furnished directly the aromatic compound **42**. The reaction of synthones **38**, **41**, and **42** with the appropriate benzoyl chloride, performed in pyridine, furnished the target compounds **8** and **11**−**33**. All the 4,7-dihydrotriazolopyrimidine derivatives were purified by crystallization from EtOH, since the compounds undergwent an extensive transformation to a main unidentified product when column chromatography was used as purification method.

Similarly to the preparation of synthones **41** and **42**, the synthesis of triazolopyrimidine-2-carboxylic acids **45** and **47** was accomplished by reacting ethyl 5-amino-1,2,4-triazole-3-carboxylate [29] with benzylideneacetone and phenyl 1-propenyl ketone, respectively, in DMF at reflux (Scheme 2). Using 3-amino-1,2,4-triazole-5-carboxylic acid as starting material, the reaction furnished only decarboxylated triazolopyrimidine scaffolds. In agreement with what has been described above, the reaction with benzylideneacetone gave the saturated compound **43**, which was then oxidized with NBS in EtOH at reflux in the presence of AcONa, to give **44**. On the other hand, the reaction with phenyl 1-propenyl ketone provided directly the aromatic intermediate **46**. Ethyl triazolopyrimidine esters **44** and **46** were then hydrolyzed under basic conditions, furnishing the key acids **45** and **47**. The carbodiimide-mediated coupling reaction was then carried out by reacting the 1,2,4-triazolopyrimidine-2-carbonyl chloride, prepared from the acids **45** and **47** by reaction with oxalyl chloride in CH_2Cl_2, with 2-amino-5,6,7,8-tetrahydro-4H-cyclohepta[b]thiophene-3-carboxamide or aniline, in CH_2Cl_2 in the presence of DIPEA, to give the target compounds **34**−**37**.

RESULTS AND DISCUSSION

Hit compound **8** (compound **31** in ref [18]), previously tested as provided from the vendor, was synthesized and retested, giving comparable results in terms of PA−PB1 interaction inhibitory activity (IC_{50} = 153 μM) and maintaining the same profile of antiviral activity and cytotoxicity. The in-house synthesized 8 was then used as comparative compound in all successive studies.

The whole set of derivatives was evaluated for the ability to inhibit the physical interaction between PA and PB1 subunits by ELISA, including the $PB1_{(1-15)}$−Tat peptide [30] as a positive control. In parallel, for all the synthesized compounds, the antiviral activity was tested by plaque reduction assay (PRA) in Mardin−Darby canine kidney (MDCK) cells infected with a reference FluA virus, the A/PR/8/34 strain. Ribavirin (RBV), a known broad-spectrum inhibitor of RNA viruses polymerase,[31] was included as a positive control of inhibition, exhibiting EC_{50} = 10 μM. To exclude that the observed antiviral activities could be due to toxic effects in the target cells, all the synthesized compounds were tested by MTT assays in two cell lines, i.e., MDCK and human embryonic kidney (HEK) 293T. The antiviral activity and toxicity data for the tested compounds are reported in Table 1.

As to what impacts the modifications made on the phenyl ring at the C-2 position of the dihydrotriazolopyrimidine core, the shifting of the methoxy group from para (compound **8**) to meta (compound **12**) and ortho (compound **11**) positions decreased the PA−PB1 interaction inhibitory activity. The same behavior was observed for the fluoro analogues **13**−**15**. Among the various para-substituted derivatives, compounds **16**−**18** were more active than hit **8**, but only for p-propoxy derivative **16** did the ability to inhibit the PA−PB1 interaction perfectly translate to anti-Flu activity in a cellular context, with EC_{50} = 47 μM. On the other hand, compounds **19**, **21**, and **25** inhibited the viral growth but did not interfere with the PA−PB1 complex formation. For these compounds, all characterized by a bulky substituent at the C-2 position, an alternative mechanism of action might be postulated, or simply the antiviral activity could be due to a certain toxicity.

The aromatic triazolopyrimidine compounds **28**−**30** were all devoid of activity against the PA−PB1 interaction, thus making them less suitable than their 4,7-dihydrotriazolopyrimidine counterparts (compounds **26**, **8**, and **16**). The Fingerprints for Ligands and Proteins (FLAP) binding poses evaluated in silico for compound **26** and its aromatic analogue **28** were very similar, with the heterocyclic and heteroaromatic cores interacting with W706 (Figure 4). However, compound **28**,

due to its more linear shape, appears to match the hydrophobic field generated by W706 less efficiently than **26**, and this difference might be responsible for the lower activity of the aromatic analogues.

When in the aromatic scaffold the methyl and phenyl groups were interchanged (compounds **31**−**33**), the PA−PB1 inhibitory activity was restored, with compound **31** exhibiting a good IC_{50} value of 26 μM, perfectly comparable to that obtained in inhibiting the vral replication (EC_{50} = 25 μM). The ability of compound **31** to interfere with PA−PB1 complex markedly decreased when the C-2 amide linker was inverted, as in compound **35**, which however maintained the antiviral activity.

Definitely, the most exciting result in this study was achieved with the hybrid molecules **36** and **37**, designed by merging some peculiar structural features of the PA−PB1 interaction inhibitors developed by us. With an IC_{50} = 1.1 μM, compound **36** emerged as the most potent PA−PB1 inhibitor within this series of compounds as well as among all the small molecules published so far. The other hybrid molecule **37**, although endowed with a lower ability to interfere with PA−PB1 complex formation (IC_{50} = 28 μM), emerged as the best in inhibiting the viral growth (EC_{50} = 8.0 μM). Structurally, the two molecules differ only in opposite positions of the substituents on the triazolopyrimidine core, with the 5-methyl group and 7-phenyl ring being the most suitable substitution pattern for PA−PB1 inhibition. To evaluate possible differences in the binding mode of compounds **36** and **37**, their FLAP binding poses were analyzed (Figure 5). Both compounds orient the triazolopyrimidine ring toward the W706 residue of PA that defines the first hydrophobic pocket, to give an efficient π−π stacking. In addition, compound **37**, due to its elongated shape, seems to be able to locate the phenyl ring into the second hydrophobic pocket of PA, defined by P710 and L666, and the cycloheptathiophene ring into the third hydrophobic pocket defined by L640, V636, and W619, according to the cavity description by Liu and co-workers33 (Figure 5A). This binding mode is comparable to that previously observed for compound **9**[24] (data not shown). On the other hand, compound **36** seems to be shifted toward the opposite side of the cavity, thus

matching only the first hydrophobic region (Figure 5B). Changing the perspective (Figure 5C,D), we can notice that, based on this model, the shift for compound **36** is due to a favored H-bonding between its 2-amidic carbonyl group and Q408, according to the FLAP GRID fields analysis. In our previous studies, the interactions with W706 and with the second hydrophobic pocket in proximity of P710 were usually detected for the most active compounds; the achievement of more active derivatives designed to optimize these hydrophobic interactions validated the hypothesis about this favorable binding mode.[22] On the contrary, compound **36** emerges as the first compound within our series of derivatives for which an interaction with Q408 seems to occur. Although these findings need to be further investigated, it is known that Q408 is a key residue for PB1 binding through H-bonding, and this might be the reason for the surprisingly potent activity. The interaction with Q408 has been recently hypothesized also for other PA−PB1 inhibitors, although their inhibitory effect was lower than that of compound **36**.[34] From the comparison of the spatial dispositions of the two amidic carbonyl groups in compounds **36** and **37** in Figures 5 with the ones in Figure 3, minor differences emerge. These differences are induced by the interaction with the protein structure, and this is a demonstration that combining a pharmacophore approach with a structure-based approach, when possible, represents a suitable strategy for pharmacophore refinement.

Compounds **16**, **31**, **36**, and **37**, endowed with the best ability to inhibit both PA−PB1 interaction and viral growth, were further characterized. First, we investigated their ability to interfere with the catalytic activity of FluA RdRP in a cellular context by minireplicon assays performed in transfected HEK 293T cells. As shown in Table 2, for all the compounds the ability to disrupt the PA−PB1 interaction in vitro correlated well with the polymerase inhibitory activity, with the best compounds **36** and **37** showing EC_{50} values of 12 and 16 μM, respectively, comparable to that of the reference compound RBV (EC_{50} = 18 μM). We then tested the ability of the best compound 36 to interfere with the physical interaction between PA and PB1 in a cellular context. To this end, we investigated whether the compound could affect PA−PB1 binding in the cell cytoplasm and consequently block the intranuclear translocation of PA, which requires formation of

a PA−PB1 complex,[32] while PB2 enters the cell nucleus independently. Thus, we transfected HEK 293T cells with plasmids expressing PB1, PB2, and a PA−GFP fusion protein and analyzed the intracellular localization of PA−GFP in the presence or absence of compound **36** (or DMSO as a control). As previously shown,[32] individually expressed PA−GFP was largely cytoplasmic, while coexpression of PA−GFP with PB1 and PB2 resulted in marked nuclear accumulation of PA (Figure 6). Treatment of PA−PB1−PB2-coexpressing cells with compound **36** reduced PA nuclear localization, while DMSO had no effect (Figure 6).

Finally, the antiviral effects of compounds **16**, **31**, **36**, and **37** against a number of strains of FluA of both HIN1 and H3N2 subtypes, including an oseltamivir-resistant clinical isolate (A/Parma/24/09), and three strains of FluB were also evaluated (Table 3). All the compounds showed an interesting antiviral activity against the whole panel of Flu strains, perfectly comparable to that measured against the A/PR/8/34 strain. Compound **37** confirmed its anti-Flu potency by exhibiting the best antiviral activity, with EC_{50} = 5 μM against both the FluA oseltamivir-resistant clinical isolate and Flu B/Lee/40 strain. At this stage, the absorption, distribution, metabolism, and excretion (ADME) profile was preliminarily determined to assess the drug-like properties of these new small molecules. Toward this end, for the same set of compounds, **16**, **31**, **36**, and **37**, along with the hit 8, the solubility (equilibrium solubility in phosphate buffer at pH 7.4), permeability (parallel artificial membrane permeation assay (PAMPA)), and human liver microsome (HLM) metabolic stability were experimentally determined. Concerning the solubility, compound **8** showed the highest equilibrium solubility (13 μg/mL), followed by compounds **16** and **31** (5 μg/mL) and then by compounds 36 and **37**, which showed very low solubility (<1 μg/mL). Because of this issue, we could not clearly estimate the cell permeability of compound **37**. Based on the PAMPA, all the tested compounds showed a medium/high permeability (data are reported in the Experimental Section) and a percentage of compound trapped into the membrane ranging from 41 to 57%, with the exception of **31**, the sole compound not retained by the lipid membrane. Notably, all the studied PA−PB1 inhibitors were metabolically stable in HLM, since no metabolites were detected after 30

min exposure to cytochrome metabolism. Altogether, these studies suggested that the triazolopyrimidine-based compounds are endowed with an adequate ADME profile for a drug-discovery phase, even though the most promising antiviral derivatives **36** and **37** suffered from low solubility. Since these hybrid molecules are made of a triazolopyrimidine core merged to a cycloheptathiophene scaffold, we hypothesize that the latter may be responsible for the low solubility. Indeed, ADME studies performed on the previous cycloheptathiophene derivatives **7** and **10** showed the same poor equilibrium solubility (<1 μg/mL) and a medium/high permeability, although they interacted almost entirely with the lipid membrane, hampering the enrichment of the acceptor phase. Thus, although compound **36** is characterized by a promising ADME profile, further modifications of the cycloheptathiophene moiety will be required to achieve the best compromise between solubility and cell permeability.

CONCLUSIONS

The limited therapeutic options against Flu infection along with the drug resistance issue make imperative the search for next generation agents. Although the inhibition of viral polymerases is a common approach in the identification of antiviral drugs, the development of compounds able to interfere with the correct assembly of viral polymerase complexes is an innovative strategy.[35−38]

In this context, we have been recently interested in the inhibition of the interaction of Flu polymerase PA−PB1 subunits by small molecules. In the present work, starting from the dihydrotriazolopyrimidine hit **8**, a weak PA−PB1 interaction inhibitor with no significant anti-Flu activity, and through a hit-to-lead optimization, novel potent inhibitors endowed with a broad anti-Flu activity have been discovered. The best results were achieved with the hybrid molecules **36** and **37**, obtained by combining the herein developed triazolopyrimidine and the previously explored cycloheptathiophene scaffolds. With an IC_{50} = 1.1 μM, compound **36** exhibits a 150-fold higher

activity than hit compound **8**, definitely emerging as the most potent in the scenario of the PA−PB1 small molecule inhibitors developed so far. This ability translates in a broad anti-Flu activity with no cytotoxicity. From this study, the triazolopyrimidine core emerges as very suitable to inhibit the physical interaction between PA and PB1 subunits, probably thanks to an efficient π–π staking interaction with W706 of the first hydrophobic pocket, as suggested by the FLAP poses. The computational studies also showed that the different binding mode of the various triazolopyrimidine derivatives is markedly influenced by the substituents at the C-5 and C-7 positions but mainly by the group placed at the C-2 position. While the 2-cycloheptanethiophene moiety is definitely able to ensure potent activity, a wider exploration of the C-2 position is strongly required, also to meet the need for compounds with an improved ADME profile. The design of new drug-like analogues, also based on hydrophilic interactions while decreasing unnecessary hydrophobic moieties, is also supported by the peculiar ability of the potent compound **36** to establish a very favored H-bonding with Q408.

During the final drafting of this manuscript, novel crystal structures of the influenza virus polymerase were published,[39,40] thus opening new opportunities to refine the SBDD.

EXPERIMENTAL SECTION

Computational methods. The binding poses in the PA cavity were generated using the FLAP software (Molecular Discovery Ltd., UK; www.moldiscovery.com). Indeed, the FLAP approach[41] was previously used to identify inhibitors of the PA-PB1 complex by virtual screening[18] and proved also to be useful to design more active compounds.[22] The procedure has been extensively described elsewhere.[22] As in the previous studies, the main cavity of the crystallographic structure of a large C-terminal fragment of PA (aa 257-716) (pdb code: 3CM8)[14] was used as a template. A total of 50 conformers for each ligand were generated to mimic the compound flexibility, and the most abundant protonation state predicted of each molecule was used, as predicted by MoKa.[42] The

probes used to generate the GRID Molecular Interaction Fields were H (shape), DRY (hydrophobic interactions), N1 (H-bond donor) and O (H-bond acceptor) interactions. The FLAP software was also used to align the selected compounds into the pharmacophore model. The pharmacophore generation using FLAPpharm algorithm[43] was recently described.[24] Here, the pharmacophore was used as a template to run the FLAP virtual screening module.

Chemistry. All reactions were routinely checked by TLC on silica gel $60F_{254}$ (Merck) and visualized by using UV or iodine. Flash column chromatography separations were carried out on Merck silica gel 60 (mesh 230-400). Melting points were determined in capillary tubes (Büchi Electrothermal Mod. 9100) and are uncorrected. HRMS spectra were registered on Agilent Technologies 6540 UHD Accurate Mass Q-TOF LC/MS, HPLC 1290 Infinity. Purities of the compounds were determined by elemental analyses and the data for C, H, and N are within ± 0.4% of the theoretical values (purity of ≥95%). Elemental analyses were performed on a Fisons elemental analyzer, Model EA1108CHN. ^{1}H NMR and ^{13}C NMR spectra were recorded at 200 MHz (Bruker Avance DPX-200) and 400 MHz (Bruker Avance DRX-400) using residual solvents such as chloroform (δ = 7.26) or dimethylsulfoxide (δ = 2.48) as an internal standard. Chemical shifts are given in ppm (δ) and the spectral data are consistent with the assigned structures. Reagents and solvents were purchased from common commercial suppliers and were used as such. After extraction, organic solutions were dried over anhydrous Na_2SO_4, filtered, and concentrated with a Büchi rotary evaporator at reduced pressure. Yields are of purified product and were not optimized. All starting materials were commercially available unless otherwise indicated.

General procedure for carbodiimide formation (Method A). A solution of the appropriate synthones (1.0 equiv) in pyridine was added of the suitable benzoyl chloride (2.0 equiv). The reaction mixture was maintained at room temperature until no starting material was detected by TCL. After cooling, the reaction mixture was poured into ice/water, obtaining a precipitate which was filtered and purified as described below.

Compounds **8** and **11-27** were prepared starting from synthone **38**[27] through Method A and purified by crystallization by EtOH.

4-Methoxy-*N*-(5-methyl-7-phenyl-4,7-dihydro[1,2,4]triazolo[1,5-*a*]pyrimidin-2-yl)benzamide (8). Yield, 100%. Light yellow crystals, mp 228-230 °C; ^{1}H NMR (DMSO-d_6) δ 1.95 (s, 3H, CH_3), 3.75 (s, 3H, OCH_3), 4.50 and 6.00 (s, each 1H, CH), 6.95 (d, J = 7.9 Hz, 2H, aromatic CH), 7.20-7.35 (m, 5 H, aromatic CH), 7.85 (d, J = 7.9 Hz, 2H, aromatic CH), 9.50 (s, 1H, NH), 10.25 (s, 1H, NHCO); ^{13}C NMR (DMSO-d_6) δ 18.7, 55.8, 59.8, 96.1, 113.9, 126.3, 127.2, 128.2, 128.9, 130.1, 131.9, 143.0, 148.9, 154.3, 162.4, 164.9. HRMS: *m/z* calcd for $C_{20}H_{19}N_5O_2$ 362.1572 and $C_{20}H_{19}N_5O_2$ H_2O 380.1678 ($M+H^+$), found 362.1619 and 380.1724. Anal. ($C_{20}H_{19}N_5O_2 \cdot 0.2$ H_2O) C, H, N.

2-Methoxy-*N*-(5-methyl-7-phenyl-4,7-dihydro[1,2,4]triazolo[1,5-*a*]pyrimidin-2-yl)benzamide (11). Yield, 94%. Light yellow crystals, mp 154-156 °C; ^{1}H NMR (DMSO-d_6) δ 1.95 (s, 3H, CH_3), 3.75 (s, 3H, OCH_3), 4.50 and 5.90 (s, each 1H, CH), 6.95 (t, J = 7.4 Hz, 1H, aromatic CH), 7.10 (d, J = 8.2 Hz, 1H, aromatic CH), 7.20-7.35 (m, 5H, aromatic CH), 7.45 (t, J = 7.4 Hz, 1H, aromatic CH), 7.55-7.65 (m, 1H, aromatic CH), 9.50 (s, 1H, NH), 10.00 (s, 1H, NHCO). Anal. ($C_{20}H_{19}N_5O_2 \cdot$ 0.3 H_2O) C, H, N.

3-Methoxy-*N*-(5-methyl-7-phenyl-4,7-dihydro[1,2,4]triazolo[1,5-*a*]pyrimidin-2-yl)benzamide (12). Yield, 75%. Light yellow crystals, mp 159-161 °C; ^{1}H NMR (DMSO-d_6) δ 1.95 (s, 3H, CH_3), 3.75 (s, 3H, OCH_3), 4.50 and 5.90 (s, each 1H, CH), 7.00-7.45 (m, 9H, aromatic CH), 9.50 (s, 1H, NH), 10.45 (s, 1H, NHCO). Anal. ($C_{20}H_{19}N_5O_2 \cdot 0.2$ H_2O) C, H, N.

4-Fluoro-*N*-(5-methyl-7-phenyl-4,7-dihydro[1,2,4]triazolo[1,5-*a*]pyrimidin-2-yl)benzamide (13). Yield, 100%. Light yellow crystals, mp 253-255 °C; ^{1}H NMR (DMSO-d_6) δ 1.95 (s, 3H, CH_3), 4.50 and 6.00 (s, each 1H, CH), 7.20-7.35 (m, 7H, aromatic CH), 7.90-7.95 (m, 2H, aromatic CH), 9.50 (s, 1H, NH), 10.50 (s, 1H, NHCO). Anal. ($C_{19}H_{16}FN_5O \cdot 0.4$ H_2O) C, H, N.

3-Fluoro-*N*-(5-methyl-7-phenyl-4,7-dihydro[1,2,4]triazolo[1,5-*a*]pyrimidin-2-yl)benzamide (14). Yield, 100%. Light yellow crystals, mp 248-250 °C; ^{1}H NMR (DMSO-d_6) δ 1.95 (s, 3H,

CH_3), 4.50 and 6.00 (s, each 1H, CH), 7.20-7.35 (m, 7H, aromatic CH), 7.45-7.55 (m, 2H, aromatic CH), 9.50 (s, 1H, NH), 10.60 (s, 1H, NHCO). Anal. ($C_{19}H_{16}FN_5O \cdot 0.5\ H_2O$) C, H, N.

2-Fluoro-*N*-(5-methyl-7-phenyl-4,7-dihydro[1,2,4]triazolo[1,5-*a*]pyrimidin-2-yl)benzamide (15). Yield, 100%. Light yellow crystals, mp 139-141 °C; ^{1}H NMR (DMSO-d_6) δ 1.95 (s, 3H, CH_3), 4.50 and 5.90 (s, each 1H, CH), 7.15-7.35 (m, 7H, aromatic CH), 7.45-7.55 (m, 2H, aromatic CH), 9.50 (s, 1H, NH), 10.50 (s, 1H, NHCO). Anal. ($C_{19}H_{16}FN_5O \cdot 0.3\ H_2O$) C, H, N.

***N*-(5-Methyl-7-phenyl-4,7-dihydro[1,2,4]triazolo[1,5-*a*]pyrimidin-2-yl)-4-propoxybenzamide (16).** Yield, 100%. Light yellow crystals, mp 235-237 °C; ^{1}H NMR (DMSO-d_6) δ 0.95 (t, J = 7.0 Hz, 3H, CH_2CH_3), 1.70 (sex, J = 7.0 Hz, 2H, CH_2CH_3), 1.90 (s, 3H, CH_3), 3.95 (t, J = 7.0 Hz, 2H, OCH_2), 4.50 and 5.95 (s, each 1H, CH), 6.90 (d, J = 8.7 Hz, 2H, aromatic CH), 7.20-7.35 (m, 5H, aromatic CH), 7.80 (d, J = 8.7 Hz, 2H, aromatic CH), 9.50 (s, 1H, NH), 10.25 (s, 1H, NHCO). Anal. ($C_{22}H_{23}N_5O_2 \cdot 0.2\ H_2O$) C, H, N.

4-Butoxy-*N*-(5-methyl-7-phenyl-4,7-dihydro[1,2,4]triazolo[1,5-*a*]pyrimidin-2-yl)benzamide (17). Yield, 45%. White crystals, mp 249-251 °C; ^{1}H NMR (DMSO-d_6) δ 0.90 (t, J = 7.4 Hz, 3H, CH_2CH_3), 1.40 (sex, J = 7.0 Hz, 2H, CH_2CH_3), 1.70 (quin, J = 6.5 Hz, 2H, $CH_2CH_2CH_3$), 1.85 (s, 3H, CH_3), 4.00 (t, J = 6.5 Hz, 2H, OCH_2), 4.50 and 5.95 (s, each 1H, CH), 6.90 (d, J = 8.5 Hz, 2H, aromatic CH), 7.20-7.35 (m, 5H, aromatic CH), 7.80 (d, J = 8.5 Hz, 2H, aromatic CH), 9.50 (s, 1H, NH), 10.25 (s, 1H, NHCO). Anal. ($C_{23}H_{25}N_5O_2 \cdot 0.2\ H_2O$) C, H, N.

4-Butyl-*N*-(5-methyl-7-phenyl-4,7-dihydro[1,2,4]triazolo[1,5-*a*]pyrimidin-2-yl)benzamide (18). Yield, 51%. White crystals, mp 261-263 °C; ^{1}H NMR (DMSO-d_6) δ 0.90 (t, J = 7.4 Hz, 3H, CH_2CH_3), 1.40 (sex, J = 7.4 Hz, 2H, CH_2CH_3), 1.70 (quin, J = 7.4 Hz, 2H, $CH_2CH_2CH_3$), 1.85 (s, 3H, CH_3), 2.55 (t, J = 7.4 Hz, 2H, CCH_2), 4.50 and 5.95 (s, each 1H, CH), 7.20-7.25 (m, 5H, aromatic CH), 7.30-7.35 (m, 2H, aromatic CH), 7.80 (d, J = 8.1 Hz, 2H, aromatic CH), 9.50 (s, 1H, NH), 10.25 (s, 1H, NHCO). Anal. ($C_{23}H_{25}N_5O \cdot 0.4\ H_2O$) C, H, N.

***N*-(5-Methyl-7-phenyl-4,7-dihydro[1,2,4]triazolo[1,5-*a*]pyrimidin-2-yl)-4-phenoxybenzamide (19).** Yield, 84%. White crystals, mp 217-219 °C; ^{1}H NMR (DMSO-d_6) δ 1.95 (s, 3H, CH_3), 4.50

and 5.90 (s, each 1H, CH), 6.90-7.40 (m, 12 H, aromatic CH), 7.90 (d, *J* = 8.4 Hz, 2H, aromatic CH), 9.55 (s, 1H, NH), 10.40 (s, 1H, NHCO). Anal. ($C_{25}H_{21}N_5O_2 \cdot 0.3\ H_2O$) C, H, N.

4-Isopropoxy-*N*-(5-methyl-7-phenyl-4,7-dihydro[1,2,4]triazolo[1,5-*a*]pyrimidin-2-yl)benzamide (20). Yield, 20%. White crystals, mp 229-231 °C; ^{1}H NMR (DMSO-d_6) δ 1.20 (d, *J* = 6.0 Hz, 6H, CH$(CH_3)_2$), 1.80 (s, 3H, CH_3), 4.50 (s, 1H, CH), 4.60 (quin, *J* = 6.0 Hz, 1H, $CH(CH_3)_2$), 5.85 (s, 1H, CH), 6.90 (d, *J* = 8.7 Hz, 2H, aromatic CH), 7.20-7.35 (m, 5H, aromatic CH), 7.80 (d, *J* = 8.7 Hz, 2H, aromatic CH), 9.55 (s, 1H, NH), 10.25 (s, 1H, NHCO). Anal. ($C_{22}H_{23}N_5O_2 \cdot 0.2\ H_2O$) C, H, N.

***N*-(5-Methyl-7-phenyl-4,7-dihydro[1,2,4]triazolo[1,5-*a*]pyrimidin-2-yl)biphenyl-4-carboxamide (21).** Yield, 56%. Light brown crystals, mp 257-259 °C; ^{1}H NMR (DMSO-d_6) δ 1.85 (s, 3H, CH_3), 4.50 and 5.90 (s, each 1H, CH), 7.20-7.45 (m, 8H, aromatic CH), 7.60-7.70 (m, 4H, aromatic CH), 7.90 (d, *J* = 8.4 Hz, 2H, aromatic CH), 9.55 (s, 1H, NH), 10.50 (s, 1H, NHCO). Anal. ($C_{25}H_{21}N_5O \cdot 0.3\ H_2O$) C, H, N.

4-Ethoxy-*N*-(5-methyl-7-phenyl-4,7-dihydro[1,2,4]triazolo[1,5-*a*]pyrimidin-2-yl)benzamide (22). Yield, 36%. Pink crystals, mp 227 °C (dec.); ^{1}H NMR (DMSO-d_6) δ 1.25 (t, *J* = 7.0 Hz, 3H, CH_2CH_3), 1.80 (s, 3H, CH_3), 4.00 (q, *J* = 7.0 Hz, 2H, CH_2CH_3), 4.50 and 5.90 (s, each 1H, CH), 6.90 (d, *J* = 8.8 Hz, 2H, aromatic CH), 7.20-7.30 (m, 5H, aromatic CH), 7.80 (d, *J* = 8.8 Hz, 2H, aromatic CH), 9.55 (s, 1H, NH), 10.25 (s, 1H, NHCO). Anal. ($C_{21}H_{21}N_5O_2 \cdot 0.5\ H_2O$) C, H, N.

***N*-(5-Methyl-7-phenyl-4,7-dihydro[1,2,4]triazolo[1,5-*a*]pyrimidin-2-yl)-4-nitrobenzamide (23).** Yield, 60%. Light yellow crystals, mp 272-274 °C; ^{1}H NMR (DMSO-d_6) δ 1.80 (s, 3H, CH_3), 4.50 and 5.90 (s, each 1H, CH), 7.15-7.30 (m, 5H, aromatic CH), 8.05 and 8.25 (d, *J* = 8.8 Hz, each 2H, aromatic CH), 9.55 (s, 1H, NH), 10.85 (s, 1H, NHCO). Anal. ($C_{19}H_{16}N_6O_3 \cdot 0.4\ H_2O$) C, H, N.

4-Chloro-*N*-(5-methyl-7-phenyl-4,7-dihydro[1,2,4]triazolo[1,5-*a*]pyrimidin-2-yl)benzamide (24). Yield, 31%. White crystals, mp 254-256 °C; ^{1}H NMR (DMSO-d_6) δ 1.80 (s, 3H, CH_3), 4.50 and 5.90 (s, each 1H, CH), 7.10-7.30 (m, 5H, aromatic CH), 7.45 and 7.80 (d, *J* = 8.8 Hz, each 2H, aromatic CH), 9.55 (s, 1H, NH), 10.55 (s, 1H, NHCO). Anal. ($C_{19}H_{16}ClN_5O \cdot 0.2\ H_2O$) C, H, N.

***N*-(5-Methyl-7-phenyl-4,7-dihydro[1,2,4]triazolo[1,5-*a*]pyrimidin-2-yl)-2-naphthamide (25).** Yield, 42%. Pink crystals, mp 230 °C (dec.); ^{1}H NMR (DMSO-d_6) δ 1.80 (s, 3H, CH_3), 4.50 and 5.90 (s, each 1H, CH), 7.20-7.30 (m, 5H, aromatic CH), 7.50-7.55 (m, 2H, aromatic CH), 7.90-8.00 (m, 4H, aromatic CH), 8.45-8.50 (m, 1H, aromatic CH), 9.55 (s, 1H, NH), 10.50 (s, 1H, NHCO). Anal. ($C_{23}H_{19}N_5O \cdot 0.3\ H_2O$) C, H, N.

***N*-(5-Methyl-7-phenyl-4,7-dihydro[1,2,4]triazolo[1,5-*a*]pyrimidin-2-yl)benzamide (26).** Yield, 18%. Light brown crystals, mp 257 °C (dec.); ^{1}H NMR (DMSO-d_6) δ 1.80 (s, 3H, CH_3), 4.50 and 5.90 (s, each 1H, CH), 7.20-7.50 (m, 8H, aromatic CH), 7.75 and 7.80 (m, 2H aromatic CH), 9.55 (s, 1H, NH), 10.50 (s, 1H, NHCO). Anal. ($C_{19}H_{17}N_5O \cdot 0.2\ H_2O$) C, H, N.

***N*-(5-Methyl-7-phenyl-4,7-dihydro[1,2,4]triazolo[1,5-*a*]pyrimidin-2-yl)-3-phenylpropanamide (27).** Yield, 9%. White crystals, mp 169-171 °C; ^{1}H NMR (DMSO-d_6) δ 1.80 (s, 3H, CH_3), 2.50 and 2.75 (t, J = 7.2 Hz, each 2H, CH_2), 4.50 and 5.90 (s, each 1H, CH), 7.00-7.25 (m, 10H, aromatic CH), 9.55 (s, 1H, NH), 10.00 (s, 1H, NHCO). Anal. ($C_{21}H_{21}N_5O \cdot 0.3\ H_2O$) C, H, N.

Compounds **28-30** were prepared starting from synthone **41**[28] through Method A and purified by flash chromatography eluting with $CHCl_3$/MeOH (98:2).

***N*-(5-Methyl-7-phenyl[1,2,4]triazolo[1,5-*a*]pyrimidin-2-yl)benzamide (28).** Yield, 19%. White crystals, mp 183-185 °C ^{1}H NMR (DMSO-d_6) δ 2.75 (s, 3H, CH_3), 7.05 (s, 1H, H-6), 7.40-7.55 (m, 6H, aromatic CH), 8.00 (d, J = 7.0 Hz, 2H, aromatic CH), 8.15-8.20 (m, 2H, aromatic CH), 9.75 (s, 1H, NHCO); ^{13}C NMR ($CDCl_3$) δ 25.1, 109.4, 127.9, 128.6, 128.9, 129.3, 129.6, 131.8, 132.2, 133.7, 146.8, 154.9, 160.0, 164.7, 165.0. HRMS: *m/z* calcd for $C_{19}H_{15}N_5O$ 330.1310 (M + H^+), found 330.1359.

4-Methoxy-*N*-(5-methyl-7-phenyl[1,2,4]triazolo[1,5-*a*]pyrimidin-2-yl)benzamide (29). Yield, 68%. White crystals, mp 190-192 °C; ^{1}H NMR (DMSO-d_6) δ 2.75 (s, 3H, CH_3), 3.80 (s, 3H, OCH_3), 6.90 (d, J = 8.8 Hz, 2H, aromatic CH) 7.05 (s, 1H, H-6), 7.50-7.55 (m, 3H, aromatic CH),

7.95 (d, *J* = 8.8 Hz, 2H, aromatic CH), 8.15-8.20 (m, 2H, aromatic CH), 9.25 (s, 1H, NHCO). Anal. ($C_{20}H_{17}N_5O_2$) C, H, N.

***N*-(5-Methyl-7-phenyl[1,2,4]triazolo[1,5-*a*]pyrimidin-2-yl)-4-propoxybenzamide (30).** Yield, 27%. White crystals, mp 180-182 °C; ^{1}H NMR (DMSO-d_6) δ 1.05 (t, *J* = 7.0 Hz, 3H, CH_2CH_3), 1.90 (sex, *J* = 7.0 Hz, 2H, CH_2CH_3), 2.75 (s, 3H, CH_3), 4.00 (t, *J* = 7.0 Hz, 2H, OCH_2), 6.90 (d, *J* = 8.8 Hz, 2H, aromatic CH) 7.05 (s, 1H, H-6), 7.55-7.65 (m, 3H, aromatic CH), 8.00 (d, *J* = 8.8 Hz, 2H, aromatic CH), 8.20-8.25 (m, 2H, aromatic CH), 9.30 (bs, 1H, NHCO). Anal. ($C_{22}H_{21}N_5O_2$) C, H, N.

Compounds **31-33** were prepared starting from synthone **42** through Method A and purified by flash chromatography eluting with $CHCl_3$/MeOH (98:2).

***N*-(7-Methyl-5-phenyl[1,2,4]triazolo[1,5-*a*]pyrimidin-2-yl)benzamide (31).** Yield, 23%. Light brown crystals, mp 217 °C (dec.); ^{1}H NMR (DMSO-d_6) δ 2.75 (s, 3H, CH_3), 7.50-7.65 (m, 6H, aromatic CH), 7.90 (s, 1H, H-6), 8.05 (d, *J* = 7.0 Hz, 2H, aromatic CH), 8.25-8.30 (m, 2H, aromatic CH), 11.50 (s, 1H, NHCO); ^{13}C NMR (DMSO-d_6) δ 17.5, 107.3, 127.8, 128.5, 128.8, 129.5, 131.5, 132.6, 134.1, 136.6, 148.2, 154.5, 159.8, 160.8, 165.3. HRMS: *m/z* calcd for $C_{19}H_{15}N_5O$ 330.1310 ($M + H^+$), found 330.1355.

4-Methoxy-*N*-(7-methyl-5-phenyl[1,2,4]triazolo[1,5-*a*]pyrimidin-2-yl)benzamide (32). Yield, 42%. White crystals, mp 210-213 °C; ^{1}H NMR (DMSO-d_6) δ 2.80 (s, 3H, CH_3), 3.85 (s, 3H, OCH_3), 7.05 (d, *J* = 8.4 Hz, 2H, aromatic CH) 7.55-7.60 (m, 3H, aromatic CH), 7.90 (s, 1H, H-6), 8.05 (d, *J* = 8.4 Hz, 2H, aromatic CH), 8.25-8.30 (m, 2H, aromatic CH), 11.25 (s, 1H, NHCO). Anal. ($C_{20}H_{17}N_5O_2$) C, H, N.

***N*-(7-Methyl-5-phenyl[1,2,4]triazolo[1,5-*a*]pyrimidin-2-yl)-4-propoxybenzamide (33).** Yield, 35%. White crystals, mp 184-186 °C; ^{1}H NMR (DMSO-d_6) δ 1.00 (t, *J* = 7.0 Hz, 3H, CH_2CH_3), 1.75 (sex, *J* = 7.0 Hz, 2H, CH_2CH_3), 2.85 (s, 3H, CH_3), 4.00 (t, *J* = 7.0 Hz, 2H, OCH_2), 7.05 (d, *J* = 8.8 Hz, 2H, aromatic CH) 7.55-7.60 (m, 3H, aromatic CH), 7.90 (s, 1H, H-6), 8.05 (d, *J* = 8.8 Hz,

2H, aromatic CH), 8.25-8.30 (m, 2H, aromatic CH), 11.25 (s, 1H, NHCO). Anal. ($C_{22}H_{21}N_5O_2$) C, H, N.

General procedure for carbodiimide formation (Method B). To a solution of the suitable carboxylic acid (1.0 equiv) in well dry CH_2Cl_2, oxalyl chloride (3 equiv) was added and after 30 min DMF (2 drops) was added. After 2 h, the reaction mixture was evaporated to dryness to give a residue that was dissolved in well dry CH_2Cl_2 and added of the appropriate aniline (1.0 equiv) and DIPEA (1.0 equiv). After 1 h, the reaction mixture was evaporated to dryness to give a residue that was treated with ice/water to give a solid that was filtered and purified as described below.

Compounds **34** and **36** were prepared starting from synthone **45** through Method B and purified by flash chromatography eluting with $CHCl_3$/MeOH (98:2) and then by crystallization by EtOH/DMF mixture.

7-Methyl-*N*,5-diphenyl[1,2,4]triazolo[1,5-*a*]pyrimidine-2-carboxamide (34). Yield, 42%. Yellow crystals, mp 186-188 °C; ^{1}H NMR ($CDCl_3$) δ 2.85 (s, 3H, CH_3), 7.15-7.20 (m, 2H, H-6 and aromatic CH), 7.40 (t, *J* = 7.9 Hz, 2H, aromatic CH), 7.60-7.65 (m, 3H, aromatic CH), 7.80 (d, *J* = 7.9 Hz, 2H, aromatic CH), 8.15-8.20 (m, 2H, aromatic CH), 9.00 (s, 1H, NHCO). HRMS: *m/z* calcd for $C_{19}H_{15}N_5O$ 330.1310 ($M + H^+$), found 330.1358. Anal. ($C_{19}H_{15}N_5O$) C, H, N.

5-Methyl-*N*,7-diphenyl[1,2,4]triazolo[1,5-*a*]pyrimidine-2-carboxamide (35). Yield, 39%. White crystals, mp 242-245 °C; ^{1}H NMR ($CDCl_3$) δ 3.00 (s, 3H, CH_3), 7.20 (t, *J* = 7.3 Hz, 1H, aromatic CH), 7.40 (t, *J* = 7.9 Hz, 2H, aromatic CH), 7.60-7.65 (m, 4H, H-6 and aromatic CH), 7.85 (d, *J* = 7.9 Hz, 2H, aromatic CH), 8.25-8.30 (m, 2H, aromatic CH), 9.50 (s, 1H, NHCO). HRMS: *m/z* calcd for $C_{19}H_{15}N_5O$ 330.1310 ($M + H^+$), found 330.1360. Anal. ($C_{19}H_{15}N_5O$) C, H, N.

N-[3-(aminocarbonyl)-5,6,7,8-tetrahydro-4H-cyclohepta[b]thien-2-yl]-7-methyl-5-phenyl[1,2,4]triazolo[1,5-a]pyrimidine-2-carboxamide (36). Yield, 30%. Yellow crystals, mp 288 °C (dec.); ^{1}H NMR (DMSO-d_6) δ 1.50-1.65 (m, 4H, cycloheptane CH_2), 1.75-1.80, (m, 2H, cycloheptane CH_2), 2.60-2.70 (m, 5H, cycloheptane CH_2 and CH_3), 2.75-2.80 (m, 2H, cycloheptane CH_2), 7.45-7.60 (m, 6H, aromatic CH, NH_2, and H-6), 8.20-8.25 (m, 2H, aromatic CH), 12.00 (s,

1H, NHCO); ^{13}C NMR (DMSO-d_6) δ 25.34, 27.5, 27.9, 28.6, 28.7, 31.9, 112.3, 122.2, 129.1, 129.7, 130.0, 131.7, 132.2, 135.6, 136.7, 147.1, 155.5, 155.9, 157.5, 167.4, 167.7. HRMS: *m/z* calcd for $C_{23}H_{22}N_6O_2S$ 447.1558 (M + H^+), found 447.1611. Anal. ($C_{23}H_{22}N_6O_2S$) C, H, N.

N-[3-(Aminocarbonyl)-5,6,7,8-tetrahydro-4H-cyclohepta[b]thien-2-yl]-5-methyl-7-phenyl[1,2,4]triazolo[1,5-a]pyrimidine-2-carboxamide (37). Yield, 25%. Orange crystals, mp 313 °C (dec.); ^{1}H NMR (DMSO-d_6) δ 1.50-1.65 (m, 4H, cycloheptane CH_2), 1.75-1.80, 2.70-2.75, and 2.80-2.85 (m, each 2H, cycloheptane CH_2), 2.90 (s, 3H, CH_3), 7.45-7.60 (m, 5H, aromatic CH and NH_2), 8.05 (s, 1H, H-6), 8.25-8.30 (m, 2H, aromatic CH), 12.00 (s, 1H, NHCO); ^{13}C NMR (DMSO-d_6) δ 17.4, 27.5, 27.9, 28.6, 28.7, 32.0, 109.2, 122.1, 128.1, 129.6, 131.8, 132.1, 135.6, 136.2, 136.7, 149.7, 155.2, 155.5, 157.9, 161.9, 167.7. HRMS: *m/z* calcd for $C_{23}H_{22}N_6O_2S$ 447.1558 (M + H^+), found 447.1601. Anal. ($C_{23}H_{22}N_6O_2S$) C, H, N.

7-Methyl-5-phenyl[1,2,4]triazolo[1,5-*a*]pyrimidin-2-amine (42). To a solution of 3,5-diamino-1,2,4-triazole (0.1 g, 0.001 mmol) in DMF (5 mL) at reflux, phenyl 1-propenyl ketone (0.14 mL, 0.001 mmol) was added and the reaction mixture was maintained at reflux for 30 min. After cooling, the mixture was evaporated to dryness, obtaining a residue that was purified by flash chromatography eluting with CH_2Cl_2/MeOH (98:2), to give **42** (0.1 g, 44%); mp 225-227 °C; ^{1}H NMR (DMSO-d_6) δ 2.60 (s, 3H, CH_3), 6.35 (s, 2H, NH_2), 7.45-7.50 (m, 3H, aromatic CH), 7.05 (s, 1H, H-6), 8.05-8.15 (m, 2H, aromatic CH); ^{13}C NMR (DMSO-d_6) δ 17.4, 105.4, 127.4, 129.3, 130.9, 137.0, 146.1, 155.1, 157.4, 167.3.

Ethyl 5-methyl-7-phenyl-4,7-dihydro[1,2,4]triazolo[1,5-a]pyrimidine-2-carboxylate (43). The title compound was prepared starting from ethyl 5-amino-1,2,4-triazole-3-carboxylate[29] and following the same procedure as used for the synthesis of **42** (2 h) using benzylideneacetone. After cooling, the reaction mixture was poured into ice/water obtaining a precipitate that was filtered and washed with Et_2O, to give **43** in 29% yield, which was used without further purification; ^{1}H NMR

(DMSO-d_6) δ 1.20 (t, J = 7.1 Hz, 3H, CH_2CH_3), 1.80 (s, 3H, CH_3), 4.20 (q, J = 7.1 Hz, 2H, CH_2CH_3), 4.55 and 6.00 (bs, each 1H, CH), 7.20-7.30 (m, 5H, aromatic CH), 9.75 (s, 1H, NH).

Ethyl 5-methyl-7-phenyl[1,2,4]triazolo[1,5-a]pyrimidine-2-carboxylate (44). To a suspension of **43** (1.4 g, 4.92 mmol) in EtOH (30 mL), NaOAc (0.59 g, 7.18 mmol) was added and the reaction mixture was heated at 40-50 °C. Then, NBS (0.87 g, 4.88 mmol) was added and the reaction mixture was refluxed for 30 min. After cooling, the reaction mixture was poured into ice/water obtaining a precipitate that was filtered and purified by flash chromatography eluting with CH_2Cl_2/MeOH (98:2), to give **44** (0.45 g, 33%); mp 174-176 °C; ^{1}H NMR ($CDCl_3$) δ 1.45 (t, J = 7.1 Hz, 3H, CH_2CH_3), 2.75 (s, 3H, CH_3), 4.50 (q, J = 7.1 Hz, 2H, CH_2CH_3), 7.15 (s, 1H, H-6), 7.55-7.65 (m, 3H, aromatic CH), 8.05-8.10 (m, 2H, aromatic CH).

5-Methyl-7-phenyl[1,2,4]triazolo[1,5-a]pyrimidine-2-carboxylic acid (45). A mixture of **44** (0.45 g, 1.59 mmol) and NaOH (0.079 g, 1.99 mmol) in MeOH (10 mL) was refluxed for 30 min. After cooling, the reaction mixture was poured into ice/water and acidified with 2N HCl obtaining a precipitate that was filtered. The filtrate was extracted with EtOAc and the organic layers were evaporated to dryness obtaining a residue that was treated with Et_2O and filtered, to give **45** (0.13 g, 32%); mp 172-174 °C; ^{1}H NMR (DMSO-d_6) δ 2.70 (s, 3H, CH_3), 7.55-7.60 (m, 4H, H-6 and aromatic CH), 8.05-8.10 (m, 2H, aromatic CH).

Ethyl 7-methyl-5-phenyl[1,2,4]triazolo[1,5-a]pyrimidine-2-carboxylate (46). The title compound was prepared starting from ethyl 5-amino-1,2,4-triazole-3-carboxylate[20] following the same procedure as used for the synthesis of **42** (1 h). After cooling, the reaction mixture was poured into ice/water and extracted with EtOAc. The organic layers were evaporated to dryness obtaining a residue that was treated with Et_2O, to give **46** in 11% yield; mp 170-172 °C; ^{1}H NMR (DMSO-d_6) δ1.30 (t, J = 7.1 Hz, 3H, CH_2CH_3), 2.80 (s, 3H, CH_3), 4.50 (q, J = 7.1 Hz, 2H, CH_2CH_3), 7.50-7.65 (m, 3H, aromatic CH), 8.05 (s, 1H, H-6), 8.15-8.25 (m, 2H, aromatic CH).

7-Methyl-5-phenyl[1,2,4]triazolo[1,5-a]pyrimidine-2-carboxylic acid (47). The title compound was prepared from **46** following the same procedure as used for the synthesis of **45** (2 h). After

cooling, the reaction mixture was evaporated to dryness obtaining a residue that was treated with ice/water and acidified with 2N HCl obtaining a precipitate that was filtered and washed with Et_2O, to give **47** in 87% yield; mp 168-169 °C; ^{1}H NMR (DMSO-d_6) δ 2.90 (s, 3H, CH_3), 7.50-7.60 (m, 3H, aromatic CH), 8.05 (s, 1H, H-6), 8.20-8.25 (m, 2H, aromatic CH).

Compounds **35** and **37** were prepared starting from synthone **47** through Method B and purified by flash chromatography eluting with $CHCl_3$/MeOH (98:2) and then by crystallization by EtOH/DMF mixture.

Biology

Compounds and peptide. RBV (1-D-ribofuranosyl-1,2,4-triazole-3-carboxamide) was obtained from Roche. Each test compound was dissolved in DMSO 100%. The $PB1_{(1–15)}$–Tat peptide was synthesized and purified by the Peptide Facility of CRIBI Biotechnology Center (University of Padua, Padua, Italy). This peptide contains the first 15 N-terminal amino acids of PB1 protein conjugated to the C-terminal sequence of HIV Tat protein (amino acids 47−59), which allows intracellular delivery.[44]

Plasmids. Plasmids pcDNA-PB1, pcDNA-PB2, pcDNA-PA, and pcDNA-NP, containing cDNA copies of the influenza A/PR/8/34 virus PB1, PB2, PA, and NP genes, respectively, were created as described elsewhere[34] and kindly provided by P. Digard (Roslin Institute, University of Edinburgh, United Kingdom). Plasmid pPolI-Flu-ffLuc, which contains an influenza virus-based luciferase minireplicon vRNA under the control of the human RNA polymerase I promoter, was provided by L. Tiley (University of Cambridge, United Kingdom). Plasmid pRL-SV40 expressing the *Renilla* luciferase was purchased from Promega. The pcDNA-PA-GFP plasmid, which encodes a PA-GFP fusion protein was kindly provided by E. Fodor (University of Oxford, United Kingdom).

Cells and Virus. Human Embryonic Kidney (HEK) 293T and Mardin-Darby canine kidney (MDCK) cells were grown in Dulbecco's modified Eagle's medium (DMEM, Life Biotechnologies) supplemented with 10% (v/v) fetal bovine serum (FBS, Life Technologies) and antibiotics (100 U/mL penicillin and 100 µg/mL streptomycin, Life Technologies). The cells were maintained at 37

°C in a humidified atmosphere with 5% CO_2. Influenza A/PR/8/34 virus (H1N1, Cambridge lineage) was obtained from P. Digard (Roslin Institute, University of Edinburgh, United Kingdom). The FluA strains A/Wisconsin/67/05 and A/Solomon Island/3/06 and the FluB strains B/Malaysia/2506/4 and B/Bangladesh/333/07 were provided by R. Cusinato (Clinical Microbiology and Virology Unit, Padua University Hospital, Padua, Italy). The clinical isolate A/Parma/24/09 was kindly provided by I. Donatelli (Istituto Superiore di Sanità, Rome, Italy). Influenza B/Lee/40 virus was obtained from W. S. Barclay (Imperial College, London, United Kingdom). All influenza viruses were propagated in MDCK cells.

PA-PB1 interaction enzyme-linked immunosorbent assay (ELISA). The PA−PB1 interaction was detected by a procedure already described.[9] Briefly, microtiter plates (Nuova Aptca) were coated with 400 ng of 6His-$PA_{(239–716)}$ for 3 h at 37 °C and then blocked with 2% BSA (Sigma) in PBS for 1 h at 37 °C. The 6His-$PA_{(239–716)}$ protein was expressed in *E. coli* strain BL21(DE3)pLysS and purified as described.[9] After washing, 200 ng of GST-PB1(1−25), or of GST alone as a control, in the absence or the presence of test compounds at various concentrations (10, 50, 100, 200 μM), were added and incubated O/N at room temperature. *Escherichia coli*-expressed, purified GST and GST-$PB1_{(1–25)}$ proteins were obtained as previously described.[9] After washing, the interaction between 6His-PA(239−716) and GST-PB1(1−25) was detected with an anti-GST monoclonal antibody conjugated to horseradish peroxidase (HRP) (GenScript). Following washes, the substrate 3,3′,5,5′tetramethylbenzidine (TMB, KPL) was added and absorbance was measured at 450 nm by an ELISA plate reader (Tecan Sunrise™). Values obtained from the samples treated with only DMSO were used to set as 100% of PA−PB1 interaction.

Cytotoxicity assay. Cytotoxicity of compounds was tested in MDCK and HEK 293T cells by the 3-(4,5-dimethylthiazol-2-yl)-2,5-diphenyl tetrazolium bromide (MTT) method, as previously reported.[9]

Plaque reduction assay (PRA). The experiments were carried out as previously described.[9] Briefly, confluent monolayers of MDCK cells were infected with FluA or FluB virus at 40

PFU/well in DMEM supplemented with 1 μg/mL of TPCK-treated trypsin (Worthington Biochemical Corporation) and 0.14% BSA and incubated for 1 h at 37°C. The influenza viruses infection was performed in the presence of different concentrations of test compounds or solvent (DMSO) as a control. Serum-free medium containing 1 μg/mL of TPCK-treated trypsin, 0.14% BSA, 1.2% Avicel, and DMSO or test compounds at the indicated concentrations was added after 1 h of virus adsorption. After 48 h of incubation, cells were fixed with 4% formaldehyde and stained with 0.1% toluidine blue. Viral plaques were counted, and the mean plaque number in the DMSO-treated control was set at 100%.

Minireplicon assay. HEK 293T cells were seeded at 10^5 per well on 24-well plates. After 24 h, cells were transfected, in the presence of test compounds at different concentrations or DMSO, with pcDNA-PB1, pcDNA-PB2, pcDNA-PA, pcDNA-NP plasmids (100 ng/well of each) along with pPolI-Flu-ffLuc plasmid (50 ng/well) as described elsewhere.[9] In addition, a plasmid constitutively expressing *Renilla* luciferase, pRL-SV40 (50 ng/well), was included in the transfection mixture to normalize variations in transfection efficiency. After 4 h, the medium was replaced with fresh DMEM containing DMSO or test compounds. At 24 h post-transfection, cells were lysed, and the relative firefly and *Renilla* luciferase activities were determined using the Dual Luciferase Assay Kit from Promega and a luminescence counter (Victor X2, PerkinElmer). The luciferase activities of the samples treated with DMSO were set as 100%.

Analysis of nuclear accumulation of the PA-PB1 complex in the presence of compound 36. HEK 293T cells were transiently transfected using the Arrest-IN™ (Biosystems) with pcDNA-PA-GFP, pcDNA-PB1, and pcDNA-PB2 in the absence or the presence of compound **36** (50 μM) or DMSO as a control. At 24 hr post-transfection, cells were fixed for 20 min with 4% formaldehyde in PBS. After permeabilization with 0.2 % Triton X-100 in PBS for 5 min at RT, cells were incubated for 20 min with TOTO-3 iodide (Molecular Probes) in PBS and 4% FBS, mounted using mounting fluid (70% glycerol in PBS), and imaged using a Leica TCS-NT/SP2 confocal

microscope equipped with a 63X oil immersion objective. Images were digitally analyzed with Leica software.

Preliminary ADME studies

Metabolic stability. The selected substrates were incubated with human liver microsomes (HLM, 0.5 mg protein/ml) (BD Biosciences) according to manufacturer's recommendations with minor modification. In summary, substrates at 5 µM final concentration were pre-incubated in a shaking water bath for 5 min at 37 °C in 100 mM potassium phosphate buffer (pH 7.4) in a total volume of 250 µL. Thus, 10 µL of a 1 mM NADPH aqueous solution were added to activate the enzymatic process. After incubation for 0 and 30 min, the addition of 250 µL of cold acetonitrile (containing 0.6 µM labetalol as internal standard) was used to terminate the reaction. Proteins were precipitated by centrifugation at 12,000 x g for 5 min at 4 °C, and aliquots of supernatants were analyzed by HPLC-MS/MS, on an Agilent 6550 UHD accurate mass Q-TOF LC/MSMS system (Agilent Technologies, Palo Alto, CA) governed by Agilent MassHunter software (B.05.01 version). The system consists of a binary pump, autosampler, thermostated column compartment, DAD detector, source and Q-TOF spectrometer. Chromatographic separation of the metabolites (Agilent 1290 UHPLC system) was performed with Agilent RRHD 1.7 µ -C18, 100 x 2.1 mm (Phenomenex USA) at a constant temperature of 40 °C. The mobile phases consisted of A: H_2O/0.1% formic acid and B: acetonitrile/0.1% formic acid at the flow of 0.45 mL/min with the following gradient: Time 0 min, B 10%; Time 6 min, B 100%. The DAD Detector stored all the acquired spectra in the 190-640 nm range (2 nm spectrum step). The ion source was an Agilent Dual JetStream operating under positive ionization mode (4000 V), with as nitrogen the desolvating gas (290 °C, 12 L/min, 35 psig). The fragmentor was set to 375 V, the skimmer to 65 V, and the octrapole RF to 750 V. The spectrometric data were collected in AutoMS/MS mode in the 100-1000 mass range, with 3 scans/sec at Collision Energy of 30 V. The TOF operated at 2 GHz.

Permeability assay. The PAMPA (Parallel Artificial Membrane Permeation Assay) method[46] was used to study permeability of compounds **8**, **16**, **31**, **36**, and **37**. In a PAMPA assay drugs permeate

by passive diffusion from the donor compartment (320 µL, Roche Teflon plate), to the acceptor compartment (280 µl, Millipore MAIPN4550), where the acceptor and the donor compartments are separated by a phospholipid coated filter (4.5 µL, Millipore MAIPN4550). Donor buffer: 0.05 M MOPSO at pH 6.5 + 0.5% (w/v) Glycocholic acid. Acceptor buffer: 0.05 M MOPSO at pH 6.5. Membrane: 10% (w/v) Egg Lecithin in Dodecane + 0.5% (w/v) Cholesterol. Permeation time was 18 h. The permeation constant, P_{eff} [10^{-6} x cm/s], and the sample distribution can be retrieved by UV analytics (SpectraMax Plus 384 Absorbance Microplate Reader, Molecular Devices) of donor (t_{start}), donor (t_{end}) and acceptor (t_{end}) using the pION PAMPA Evolution software. According to this method, low permeability is expected when $P_{eff} < 0.2 \times 10^{-6}$ cm/s and Membrane% < 20%, where P_{eff} represents the effective permeability and Membrane% represents the percentage of compounds trapped into the membrane. When one or both parameters are above the cut-off then a medium to high permeability is expected (compound **8**: $P_{eff} = 3.52 \times 10^{-6}$ cm/s and Membrane% = 57%; compound **16**: $P_{eff} = 2.93 \times 10^{-6}$ cm/s and Membrane% = 41%; compound **31**: $P_{eff} = 5.49 \times 10^{-6}$ cm/s and Membrane% = 2%; compound **36**: $P_{eff} = 0.61 \times 10^{-6}$ cm/s and Membrane% = 45%; compound **37**: undetected; compound **7**: $P_{eff} = 0.00 \times 10^{-6}$ cm/s and Membrane% = 99%; compound **10**: $P_{eff} = 0.00 \times 10^{-6}$ cm/s and Membrane% = 98%).

Equilibrium solubility in aqueous media. An accurately weighted amount of compound (about 1 mg) as dry powder was placed in a glass tube and 330 µL of 0.15 M Phosphate buffer at pH 7.4 were added. Thus, the sample was ultrasonicated for 1 hour, shaken at room temperature for 2 hours (Branson 1210, Branson Ultrasonics, Danbury, CT) and let stand to equilibrate overnight. The next day, the pH of the sample was checked and the solution was filtered using a MultiScreenHTS-PCF filter (Millipore, Darmstadt, Germany). Aliquots of the filtrate were used to generate three different samples (undiluted, diluted as 1:10 and as 1:100) by dilution with the same buffer. Compound calibration curves were generated from standard 1 mg/mL DMSO solutions diluted in buffer. Calibration standards and samples were then analyzed by LC-UV.MS using an Agilent 1260 Infinity HPLC-MS system (Agilent Technologies, Santa Clara, CA) equipped with a DAD detector

and an API single quadruple mass spectrometer (Agilent 6140, Santa Clara, CA). A Kinetex XB 2.6 µm, 2.1 x 50 mm analytical column (Phenomenex, Torrance, CA) operating at 60 °C was used. The mobile phase consisted of A (water) and B (acetonitrile), both containing 0.1 %/vol formic acid. The gradient elution was performed with a flow rate of 1.5 mL/min using a generic fast gradient. After detection with DAD, the eluent entered the electrospray system using the following source settings: capillary voltage + 3.5 kV, drying gas flow (N2) 13 L/min, nebulizer pressure 60 sig, drying gas temperature 350 °C. The integral of the pseudo molecular ion intensity, [M+H]+, was acquired in single reaction monitoring mode (SRM).

ASSOCIATED CONTENT

Supporting information

Table containing Elemental Analysis data for target compounds **8** and **11-37**. This material is available free of charge via the Internet at http://pubs.acs.org.

AUTHOR INFORMATION

Corresponding Authors

For OT: phone, + 39 075 585 5139; fax, +39 075 585 5115; e-mail, oriana.tabarrini@unipg.it. For LG: phone, +39 075 585 5632; fax, +39 075 45646; e-mail, laura.goracci@unipg.it. For AL: phone, +39 049 8272363; fax, +39 049 8272355; e-mail, arianna.loregian@unipd.it.

Author contributions

⊥There are two sets of equal contributions: (1) S.M. and G.N. contributed equally to this work; (2) A.L. and O.T. contributed equally to this work.

Notes

The authors declare no competing financial interest.

ACKNOWLEDGEMENTS

We thank P. Digard, R. Cusinato, Donatelli, and W. S. Barclay for FluA and FluB viruses; P. Digard, E. Fodor, and L. Tiley for plasmids. We also thank R. Alvarez, S. Wendelspiess, and V. Micallef at F. Hoffmann-La Roche Ltd. for permeability and solubility assays. This work was supported by Italian Ministry of Health and Istituto Superiore Sanità, Progetto Finalizzato 2009 "Studio e Sviluppo di Nuovi Farmaci Antivirali Contro Infezioni da Virus Influenzale AH1N1" (to V.C., A.L., G.P., and O.T.), and by ESCMID Research Grant 2013 (to B.M.).

ABBREVIATIONS USED

ADME, absorption, distribution, metabolism and excretion; CC_{50}, concentration that causes a decrease of cell viability by 50%; Flu, influenza virus; FluA, influenza A virus; FluB, influenza B virus; HEK, human embryonic kidney; HLM, human liver microsomes; MDCK, Mardin-Darby canine kidney; PA, polymerase acidic protein; PAMPA, parallel artificial membrane permeability assay; PB1, polymerase basic protein 1; PB2, polymerase basic protein 2; PPI, protein-protein interaction; PRA, plaque reduction assays; RBV, Ribavirin; RdRP, RNA-dependent RNA polymerase.

REFERENCES

1. Ison, M. G. Clinical Use of Approved Influenza Antivirals: Therapy and Prophylaxis. *Influenza Other Respir. Viruses* **2013**, *1*, 7−13.
2. Pielak, R. M.; Chou, J. J. Flu Cannel Drug Resistance: a Tale of Two Sites. *Protein Cell.* **2010**, *1*, 246−258.
3. Samson, M.; Pizzorno, A.; Abed, Y.; Boivin, G. Influenza Virus Resistance to Neuraminidase Inhibitors. *Antiviral Res*. **2013**, *98*, 174−185.

4. Bright, R. A.; Shay, D. K.; Shu, B.; Cox, N. J.; Klimov, A. I. Adamantane Resistance Among Influenza A Viruses Isolated Early During the 2005–2006 Influenza Season in the United States. *JAMA* **2006**, *295*, 891–894.
5. de Jong, M. D.; Tran, T. T.; Truong, H. K.; Vo, M. H.; Smith, G. J.; Nguyen, V. C.; Bach, V. C.; Phan, T. Q.; Do, Q. H.; Guan, Y.; Peiris, J. S.; Tran, T. H.; Farrar, J. Oseltamivir Resistance During Treatment of Influenza A (H5N1) Infection. *N. Engl. J. Med.* **2005**, *353*, 2667-2672.
6. Resa-Infante, P.; Jorba, N.; Coloma, R.; Ortin, J. The Influenza Virus RNA Synthesis Machine: Advances in its Structure and Function. *RNA Biol.* **2011**, *8*, 207-215.
7. Loregian, A.; Palù, G. Disruption of Protein-Protein Interactions: Towards New Targets for Chemotherapy. *J. Cell. Physiol.* **2005**, *204*, 750-762.
8. Palù, G.; Loregian, A. Inhibition of Herpesvirus and Influenza Virus Replication by Blocking Polymerase Subunit Interactions. *Antiviral Res.* **2013**, *99*, 318-327.
9. Loregian, A.; Mercorelli, B.; Nannetti, G.; Compagnin, C.; Palù, G. Antiviral Strategies Against Influenza Virus: Towards New Therapeutic Approaches. *Cell. Mol. Life Sci.* **2014**, *71*, 3659-3683.
10. Perez, D.R. and Donis, R.O. A 48-amino-acid region of influenza A virus PB1 protein is sufficient for complex formation with PA. *J Virol*. **1995**, *69*, 6932-6939.
11. González S, Zürcher T, Ortín J. Identification of two separate domains in the influenza virus PB1 protein involved in the interaction with the PB2 and PA subunits: a model for the viral RNA polymerase structure. *Nucleic Acids Res*. ***1996***, *24*, 4456-4463.
12. Perez, D.R. and Donis, R.O. Functional analysis of PA binding by influenza a virus PB1: effects on polymerase activity and viral infectivity. *J Virol.* **2001**, *75*, 8127-8136.
13. Obayashi, E.; Yoshida, H.; Kawai, F.; Shibayama, N.; Kawaguchi, A.; Nagata, K.; Tame, J. R.; Park, S. Y. The structural basis for an essential subunit interaction in influenza virus RNA polymerase. *Nature* **2008**, *454*, 1127-1131.

14. He, X.; Zhou, J.; Bartlam, M.; Zhang, R.; Ma, J.; Lou, Z.; Li, X.; Li, J.; Joachimiak, A.; Zeng, Z.; Ge, R.; Rao, Z.; Liu, Y. Crystal Structure Of The Polymerase PA(C)-PB1(N) Complex From An Avian Influenza H5N1 Virus. *Nature* **2008**, *454*, 1123-1126.
15. Sugiyama, K.; Obayashi, E.; Kawaguchi, A.; Suzuki, Y.; Tame, J. R.; Nagata, K.; Park, S. Y. Structural insight into the essential PB1–PB2 subunit contact of the influenza virus RNA polymerase. *EMBO J.* **2009**, *28*, 1803–1811.
16. Li, C.; Ba, Q.; Wu, A.; Zhang, H.; Deng, T.; Jiang, T. A Peptide Derived from the C-Terminus of PB1 Inhibits Influenza Virus Replication by Interfering with Viral Polymerase Assembly. *FEBS J.* **2013**, *280*, 1139-1149.
17. Chase, G.; Wunderlich, K.; Reuther, P.; Schwemmle, M. Identification of Influenza Virus Inhibitors which Disrupt of Viral Protein-protein Interactions. *Methods* **2011**, *55*, 188–191.
18. Muratore, G.; Goracci, L.; Mercorelli, B.; Foeglein, Á.; Digard, P.; Cruciani, G.; Palù, G.; Loregian, A. Small Molecule Inhibitors of Influenza A and B Viruses that Act by Disrupting Subunit Interactions of the Viral Polymerase. *Proc. Natl. Acad. Sci. USA* **2012**, *109*, 6247-6252.
19. Fukuoka, M.; Minakuchi, M.; Kawaguchi, A.; Nagata, K.; Kamatari, Y.O.; Kuwata, K. Structure-Based Discovery of Anti-Influenza Virus A Compounds Among Medicines. *Biochim. Biophys. Acta* **2012**, *1820*, 90-95.
20. Muratore, G.; Mercorelli, B.; Goracci, L.; Cruciani, G.; Digard, P.; Palù, G.; Loregian, A. The Human Cytomegalovirus Inhibitor AL18 also Possesses Activity Against Influenza A and B Viruses. *Antimicrob. Agents Chemother*. **2012**, *56*, 6009-6013.
21. Kessler, U.; Castagnolo, D.; Pagano, M.; Deodato, D.; Bernardini, M.; Pilger, B.; Ranadheera, C.; Botta, M. Discovery and Synthesis of Novel Benzofurazan Derivatives as Inhibitors of Influenza A Virus. *Bioorg. Med. Chem. Lett*. **2013**, *23*, 5575-5577.
22. Massari, S.; Nannetti, G.; Goracci, L.; Sancineto, L.; Muratore, G.; Sabatini, S.; Manfroni, G.; Mercorelli, B.; Cecchetti, V.; Facchini, M.; Palù, G.; Cruciani, G.; Loregian, A.; Tabarrini, O.

Structural Investigation of Cycloheptathiophene-3-carboxamide Derivatives Targeting Influenza Virus Polymerase Assembly. *J. Med. Chem*. **2013**, *56*, 10118-10131.

23. Pagano, M.; Castagnolo, D.; Bernardini, M.; Fallacara, A. L.; Laurenzana, I.; Deodato, D.; Kessler, U.; Pilger, B.; Stergiou, L.; Strunze, S.; Tintori, C.; Botta, M. The Fight Against the Influenza A Virus H1N1: Synthesis, Molecular Modeling, and Biological Evaluation of Benzofurazan Derivatives as Viral RNA Polymerase Inhibitors. *ChemMedChem* **2014**, 9, 129-150.
24. Lepri, S.; Nannetti, G.; Muratore, G.; Cruciani, G.; Ruzziconi, R.; Mercorelli, B.; Palù, G.; Loregian, A.; Goracci, L. Optimization of Small-Molecule Inhibitors of Influenza Virus Oolymerase: from Thiophene-3-carboxamide to Polyamido Scaffolds. *J. Med. Chem*. **2014**, *57*, 4337-4350
25. Loregian, A.; Mercorelli, B.; Nannetti, G.; Compagnin, C.; Palù, G. Antiviral Strategies Against Influenza Virus: Towards New Therapeutic Approaches. *Cell. Mol. Life Sci.* **2014**, *71*, 3659-3683.
26. El Ashry, E. S. H.; Rashed, N. 1, 2,4-Triazolo- and tetrazolo[x,y-z]pyrimidine. *Adv. Heterocycl. Chem.* **1998**, *72*, 127-224.
27. Lipson, V.V.; Desenko, S. M.; Orlov, V. D.; Shishkin, O. V.; Shirobokova, M. G.; Chernenko, V. N.; Zinov'eva, L. I. Cyclocondensation of 3-Amino-1,2,4-triazoles with Esters of Substituted Cinnamic Acids and Aromatic Unsaturated ketones. *Chem. Het. Comp.* **2000**, *36*, 1329-1335.
28. Chernyshev, V. M.; Sokolov, A. N.; Taranushich, V. A. Improved Synthesis of 2-Amino-1,2,4-triazolo[1,5-*a*]pyrimidines. *Russ. J. Appl. Chem.* **2006**, *79*, 1134-1137.
29. Cherneyshev, V. M.; Chernysheva, A. V.; Taranushich, V. A. Synthesis of Esters and Amides of 5-Amino-1,2,4-triazole-3-carboxylic and 5-Amino-1,2,4-triazol-3-ylacetic Acids. *Russ. J. Appl. Chem.* **2006**, *79*, 783-786.

30. Wunderlich, K.; Mayer, D.; Ranadheera, C.; Holler, A.S.; Mänz, B.; Martin, A.; Chase, G.; Tegge, W.; Frank, R.; Kessler, U.; Schwemmle, M. Identification of a PA-binding Peptide with Inhibitory Activity Against Influenza A and B Virus Replication. *PLoS One* **2009**, *4*, e7517.
31. Sidwell, R. W.; Huffman, J. H.; Khare, G. P.; Allen, L. B.; Witkowski, J. T.; Robins, R. K. Broad-Spectrum Antiviral Activity of Virazole: 1-Beta-D-ribofuranosyl-1,2,4-triazole-3-carboxamide. *Science* **1972**, *177*, 705-706.
32. Fodor, E., Smith, M. The PA subunit is required for efficient nuclear accumulation of the PB1 subunit of the influenza A virus RNA polymerase complex. *J Virol.* **2004**, 78: 9144–9153.
33. Liu, H.; Yao, X. Molecular Basis of the Interaction for an Essential Subunit PA-PB1 in Influenza Virus RNA Polymerase: Insights from Molecular Dynamics Simulation and free Energy Calculation. *Mol. Pharm.* **2010**, *7*, 75–85.
34. Tintori, C.; Laurenzana, I.; Fallacara, A. L.; Kessler, U.; Pilger, B.; Stergiou, L.; Botta, M. High-Throughput Docking for the Identification of New Influenza A Virus Polymerase Inhibitors Targeting the PA-PB1 Protein-Protein Interaction. *Bioorg. Med. Chem. Lett*. **2014**, *24*, 280-282.
35. Loregian, A.; Marsden, H. S.; Palù, G. Protein-protein Interactions as Targets for Antiviral Chemotherapy. *Rev. Med. Virol.* **2002**, *12*, 239-262.
36. Loregian, A.; Palù, G. Disruption of the Interactions Between the Subunits of Herpesvirus DNA Polymerases as a Novel Antiviral Strategy. *Clin. Microbiol. Infect.* **2005**, *11*, 437-446.
37. Loregian, A.; Coen, D. M. Selective Anti-cytomegalovirus Compounds Discovered by Screening for Inhibitors of Subunit Interactions of the Viral Polymerase. *Chem. Biol.* **2006**, *13*, 191-200.
38. Pilger, B. D.; Cui, C.; Coen, D. M. Identification of a Small Molecule that Inhibits Herpes Simplex Virus DNA Polymerase Subunit Interactions and Viral Replication. *Chem. Biol.* **2004**, *11*, 647-654.

39. Pflug, A.; Guilligay, D.; Reich, S.; Cusack, S. Structure of influenza A polymerase bound to the viral RNA promoter. Nature, **2014**, *516*, 355–360.

40. Reich, S.; Guilligay, D.; Pflug, A.; Malet, H.; Berger, I.; Crépin, T.; Hart, D.; Lunardi, T.; Nanao, M.; Ruigrok, R.W.; Cusack, S. Structural insight into cap-snatching and RNA synthesis by influenza polymerase. Nature, **2014**, *516*, 361-366.

41. Baroni, M.; Cruciani, G.; Sciabola, S.; Perruccio, F.; Mason, J. S. A common reference framework for analyzing/comparing proteins and ligands. Fingerprints for Ligands and Proteins (FLAP): Theory and Application. *J. Chem. Inf. Model* **2007**, *47*, 279-294.

42. Cruciani, G.; Milletti, F.; Storchi, L.; Sforna, G.; Goracci, L., In Silico pKa Prediction in ADME Profiling. *Chem. Biodivers.* **2009**, *6*, 1812-1821.

43. Cross, S.; Baroni, M.; Goracci, L.; Cruciani, G. GRID-Based Three-Dimensional Pharmacophores I: FLAPpharm, a Novel Approach for Pharmacophore Elucidation. *J. Chem. Inf. Model.* **2012**, *52*, 2587−2598.

44. Fawell, S.; Seery, J.; Daikh, Y.; Moore, C.; Chen, L.L.; Pepinsky, B.; Barsoum, J. Tat-Mediated Delivery of Heterologous Proteins Into Cells. *Proc. Natl. Acad. Sci. USA* **1994**, *91*, 664-668.

45. Mullin, A. E.; Dalton, R. M.; Amorim, M. J.; Elton, D.; Digard, P. Increased Amounts of the Influenza Virus Nucleoprotein do not Promote Higher Levels of Viral Genome Replication. *J. Gen. Virol.* **2004**, *85*, 3689-3698.

46. Kansy, M.; Senner, F.; Gubernator, K. Physicochemical High Throughput Screening: Parallel Artificial Membrane Permeation Assay in the Description of Passive Absorption Processes. *J. Med. Chem.* **1998**, *41*, 1007-1010.

Table 1. Structure and Biological Activity of the Compounds Synthesized in This Study.

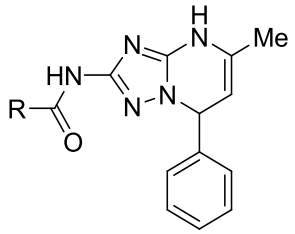

Compd	R	ELISA PA-PB1 Interaction Assay IC_{50}, μM[a]	PRA in MDCK cells EC_{50}, μM[b]	Cytotoxicity (MTT Assay) HEK 293T cells CC_{50}, μM[c]	Cytotoxicity (MTT Assay) MDCK cells CC_{50}, μM[c]
8	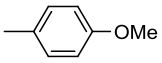	153 ± 35	>100	>250	240 ± 19
11	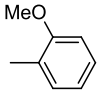	>200	>100	240 ± 27	>250
12	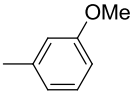	175 ± 17	>100	230 ± 17	>250
13	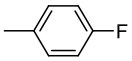	138 ± 17	>100	190 ± 11	>250
14	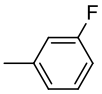	156 ± 6	>100	220 ± 13	>250
15		185 ± 12	>100	>250	>250
16	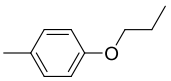	40 ± 3	47 ± 5	>250	230 ± 22
17	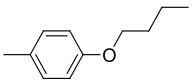	37 ± 4	100 ± 16	>250	196 ± 15
18	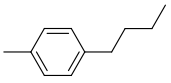	48 ± 7	100 ± 7	>250	>250
19	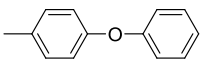	156 ± 18	59 ± 3	73 ± 6	180 ± 15
20	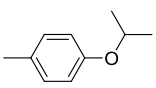	75 ± 5	>100	>250	>250
21	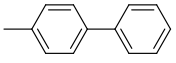	>200	28 ± 2	155 ± 16	193 ± 21

22	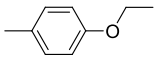	139 ± 23	100 ± 8	237 ± 14	>250
23	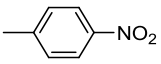	75 ± 5	>100	>250	>250
24	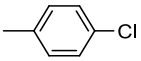	95 ± 13	>100	>250	>250
25	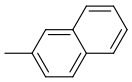	>200	41 ± 1	154 ± 15	115 ± 10
26		100 ± 10	100 ± 13	>250	>250
27	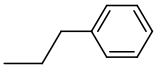	100 ± 20	>100	223 ± 19	>250
	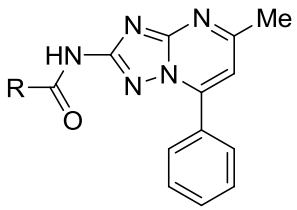				
28		>200	>100	>250	>250
29	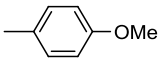	>200	86 ± 4	187 ± 14	>250
30	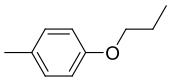	>200	>100	95 ± 6	72 ± 9
	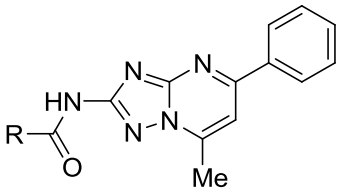				
31		26 ± 5	25 ± 1	196 ± 11	>250
32	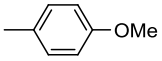	150 ± 11	>100	109 ± 16	>250
33	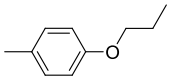	158 ± 14	>100	52 ± 2	247 ± 3

	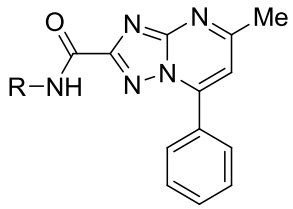				
34		160 ± 11	42 ± 5	110 ± 15	>250
36	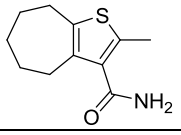	1.1 ± 0.3	21 ± 4	>250	>250
	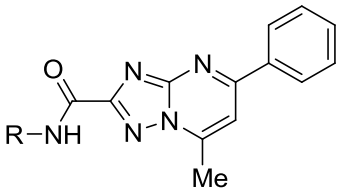				
35		128 ± 15	49 ± 2	>250	>250
37	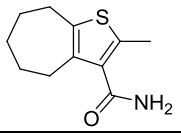	28 ± 1	8 ± 2	>250	>250
RBV			10 ± 2	>250	>250
Tat-PB1$_{1\text{-}15}$ peptide		35 ± 3	40 ± 5	>100	>100

[a] Activity of the compounds in ELISA PA-PB1 interaction assays. The IC_{50} value represents the compound concentration that reduces by 50% the interaction between PA and PB1. [b] Activity of the compounds in plaque reduction assays with the FluA A/PR/8/34 strain. The EC_{50} value represents the compound concentration that inhibits 50% of plaque formation. [c] Activity of the compounds in MTT assays. The CC_{50} value represents the compound concentration that causes a decrease of cell viability of 50%. All the reported values represent the means ± SD of data derived from at least three independent experiments in duplicate.

Table 2. Activity of Selected Compounds Against FluA RNA Polymerase Activity.

Compound	FluA Minireplicon Assay (EC_{50}, μM)[a]
16	38 ± 2
31	35 ± 7

36	12 ± 1
37	16 ± 5
RBV	18 ± 4

[a] The EC_{50} value represents the compound concentration that reduces by 50% the activity of FluA virus RNA polymerase in 293T cells. All data shown represent the means ± SD of data derived from at least three independent experiments in duplicate.

Table 3. Activity of Selected Compounds Against a Panel of FluA and FluB Strains.

Virus strain	Compound PRA (EC_{50}, μM)[a]			
	16	**31**	**36**	**37**
A/PR/8/34 (H1N1)	47 ± 5	25 ± 1	21 ± 4	8 ± 2
A/Solomon Island/3/06 (H1N1)	27 ± 3	27 ± 2	23 ± 4	16 ± 4
A/Parma/24/09 (H1N1) (Oseltamivir-resistant)	49 ± 7	25 ± 3	25 ± 2	5 ± 1
A/Wisconsin/67/05 (H3N2)	37 ± 6	24 ± 2	7 ± 1	14 ± 3
B/Lee/40	51 ± 6	25 ± 2	24 ± 4	5 ± 1
B/Malaysia/2506/04	32 ± 2	36 ± 3	17 ± 2	11 ± 3
B/Bangladesh/333/07	27 ± 4	34 ± 2	11 ± 1	12 ± 2

[a] The EC_{50} value represents the compound concentration that inhibits 50% of plaque formation. All data shown represent the means ± SD of data derived from at least three independent experiments.

Figure legends

Figure 1. Small molecules RNA-dependent RNA polymerase PA-PB1 interaction inhibitors. For the definition of IC_{50}, EC_{50}, and CC_{50} values, see Table 1.

Figure 2. Pharmacophore model for PA-PB1 inhibitors (A) and alignment of **28** (B) and **31** (C) on it using FLAP. Color code for the pharmacophore points: green = hydrophobic; red = H-bond acceptor; blue = H-bond donor.

Figure 3. Alignment of **36** (A) and **37** (B) to the pharmacophore model.

Figure 4. FLAP binding poses for compounds **26** (A) and **28** (B). A detail of the interaction of the two compounds with W706 is also reported (C). The GRID hydrophobic regions (green) generated using the FLAP software are displayed,[29] together with some of the PA key residues located in the cavity.

Figure 5. FLAP binding poses for compounds **36** (B, D) and **37** (A, C). Two different orientations in the PA cavity are reported for each compound, to better visualize the hypothesized interactions.

Figure 6. Effects of compound 36 on PA-PB1 interaction in cells. HEK 293T cells were transfected with plasmids expressing PB1, PB2, and a PA-GFP fusion protein in the absence or the presence of compound **36** or DMSO as a control. Non-transfected cells (None) and cells transfected with the PA-GFP-expressing plasmid alone served as negative controls. At 24 hr post-transfection, cells were examined by confocal laser scanning microscopy. Individual blue (TOTO-3 iodide) and green (GFP) channels are shown, with merged images on the right.

Scheme Footnotes

Scheme 1[a]

[a] Reagents and conditions: (i) DMF, reflux; (ii) pyridine; (iii) DMF, Ac_2O, reflux; (iv) AcONa, NBS, EtOH, reflux; (v) 12N HCl, EtOH, reflux.

Scheme 2[a]

[a] Reagents and conditions: (i) DMF, reflux; (ii) AcONa, NBS, EtOH, reflux; (iii) NaOH, MeOH, reflux; (iv) 1) oxalyl chloride, CH_2Cl_2, DMF; 2) $R'NH_2$, CH_2Cl_2, DIPEA.

Figure 1.

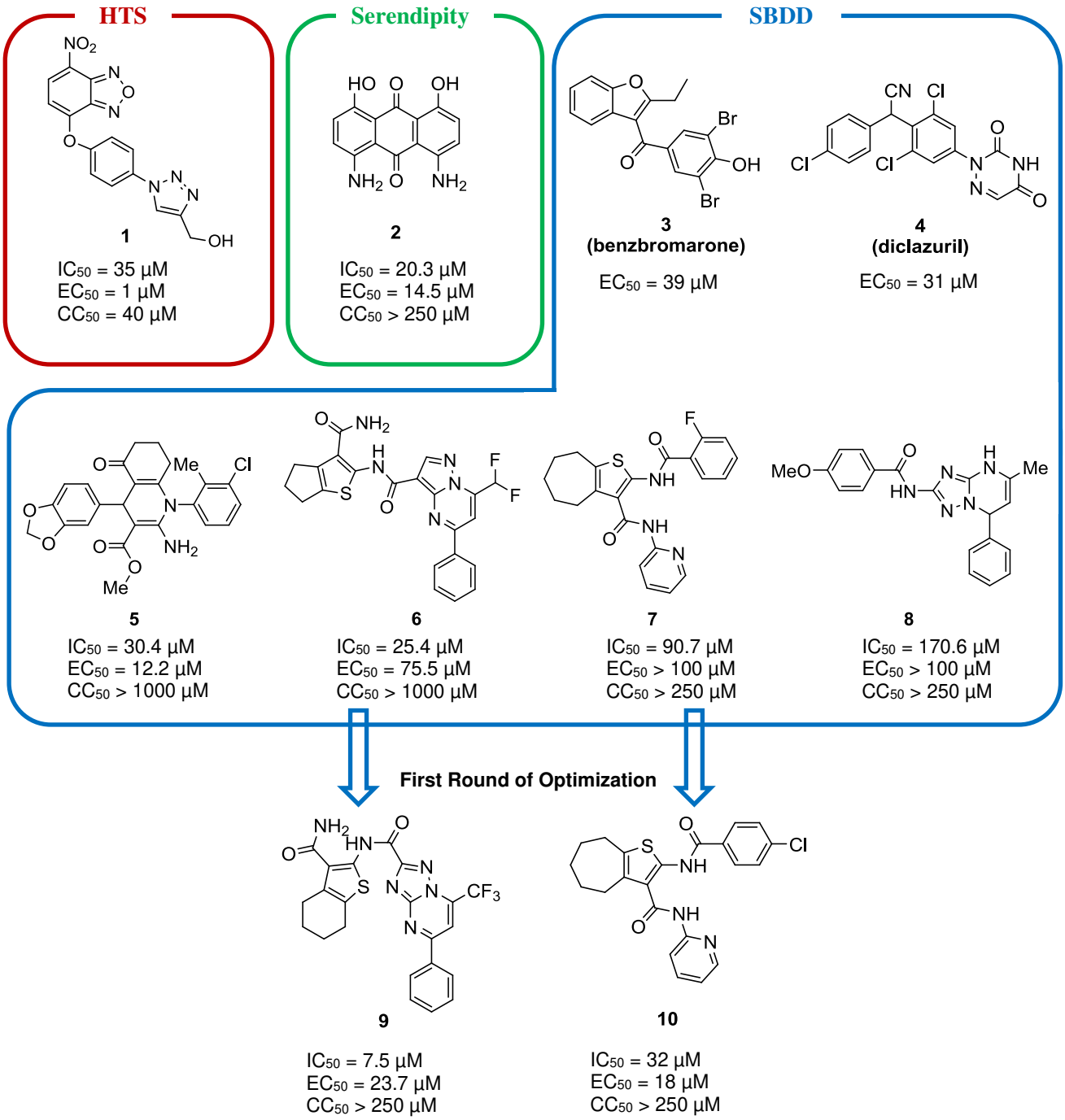
HTS
Serendipity
SBDD
1
IC50 = 35 μM
EC50 = 1 μM
CC50 = 40 μM
2
IC50 = 20.3 μM
EC50 = 14.5 μM
CC50 > 250 μM
3
(benzbromarone)
EC50 = 39 μM
4
(diclazuril)
EC50 = 31 μM
5
IC50 = 30.4 μM
EC50 = 12.2 μM
CC50 > 1000 μM
6
IC50 = 25.4 μM
EC50 = 75.5 μM
CC50 > 1000 μM
7
IC50 = 90.7 μM
EC50 > 100 μM
CC50 > 250 μM
8
IC50 = 170.6 μM
EC50 > 100 μM
CC50 > 250 μM
First Round of Optimization
9
IC50 = 7.5 μM
EC50 = 23.7 μM
CC50 > 250 μM
10
IC50 = 32 μM
EC50 = 18 μM
CC50 > 250 μM

Figure 2.

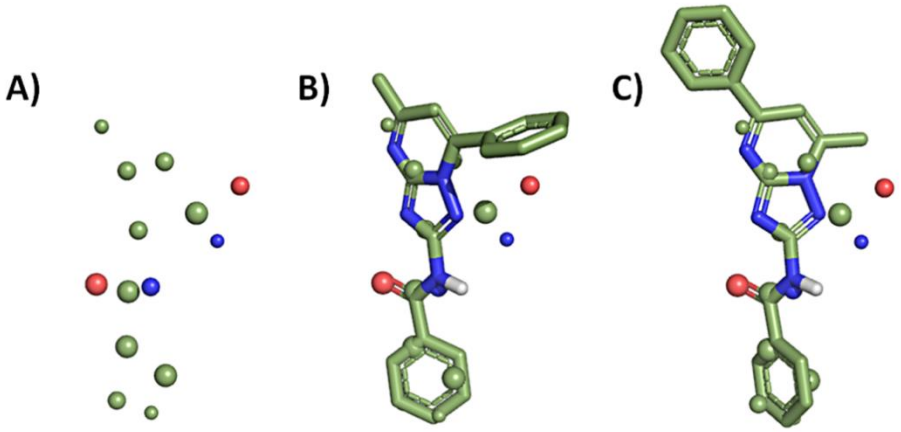

Figure 3.

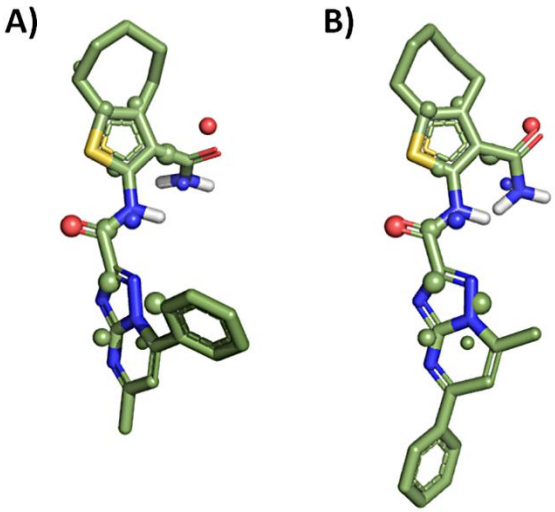

Figure 4.

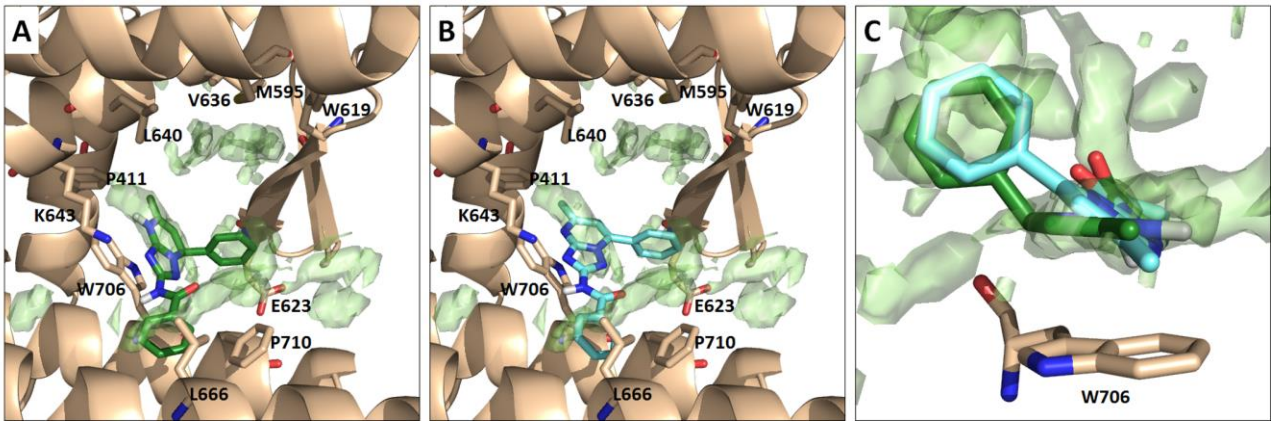

Figure 5.

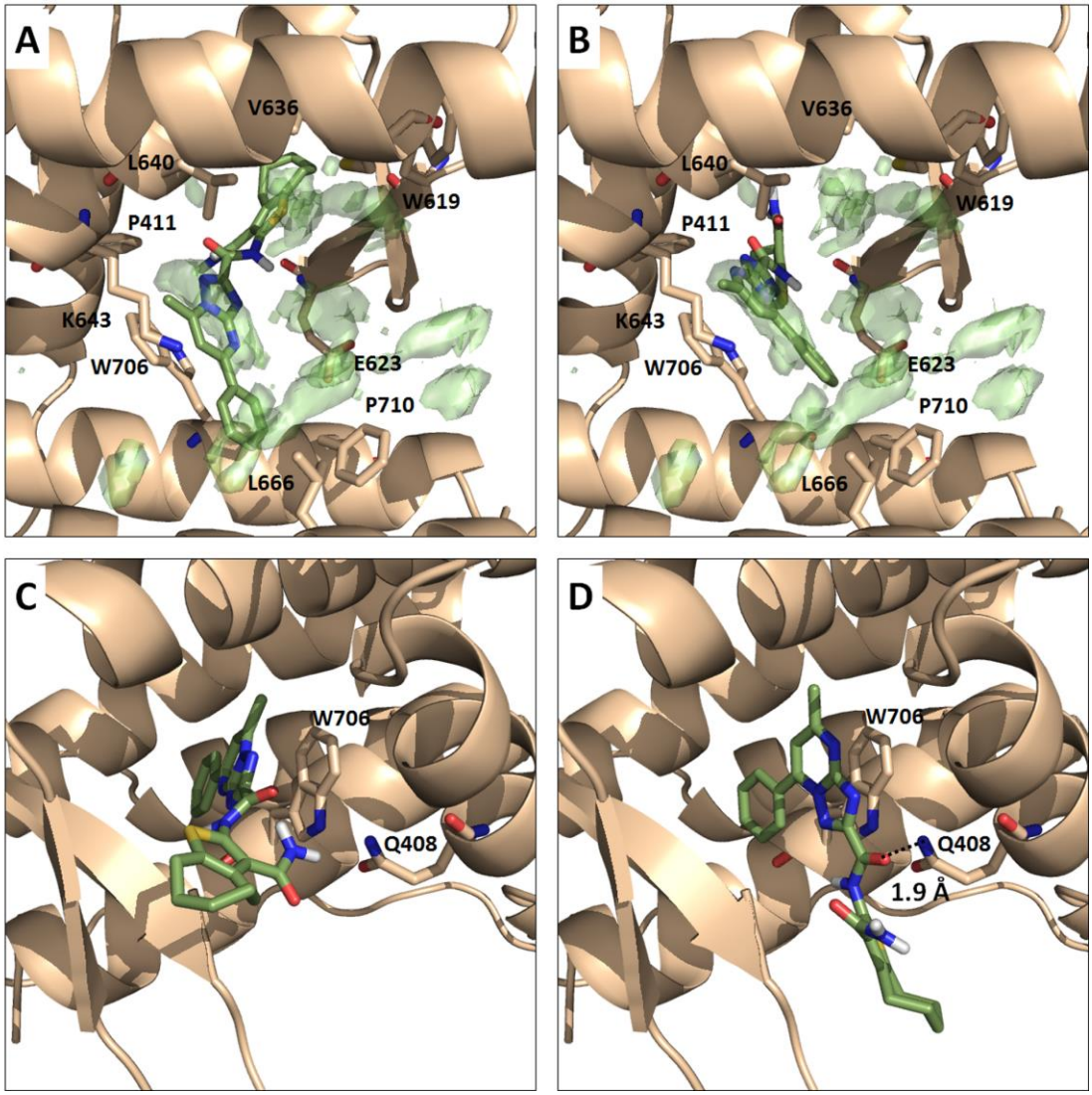
A
V636
L640
W619
P411
K643
W706
E623
P710
L666
B
V636
L640
W619
P411
K643
W706
E623
P710
L666
C
W706
Q408
D
W706
Q408
1.9 Å

Figure 6.

Scheme 1[a]

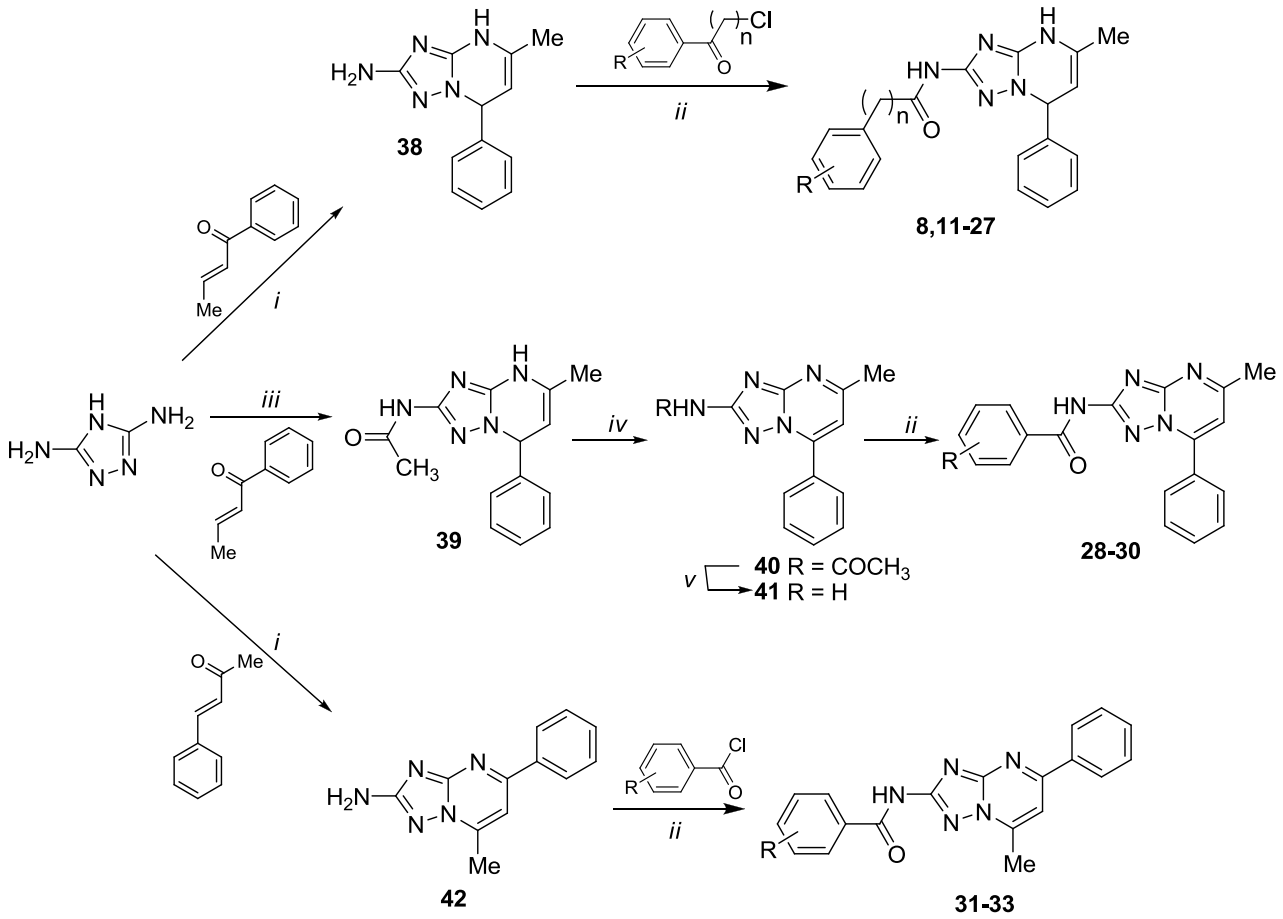

Scheme 2[a]

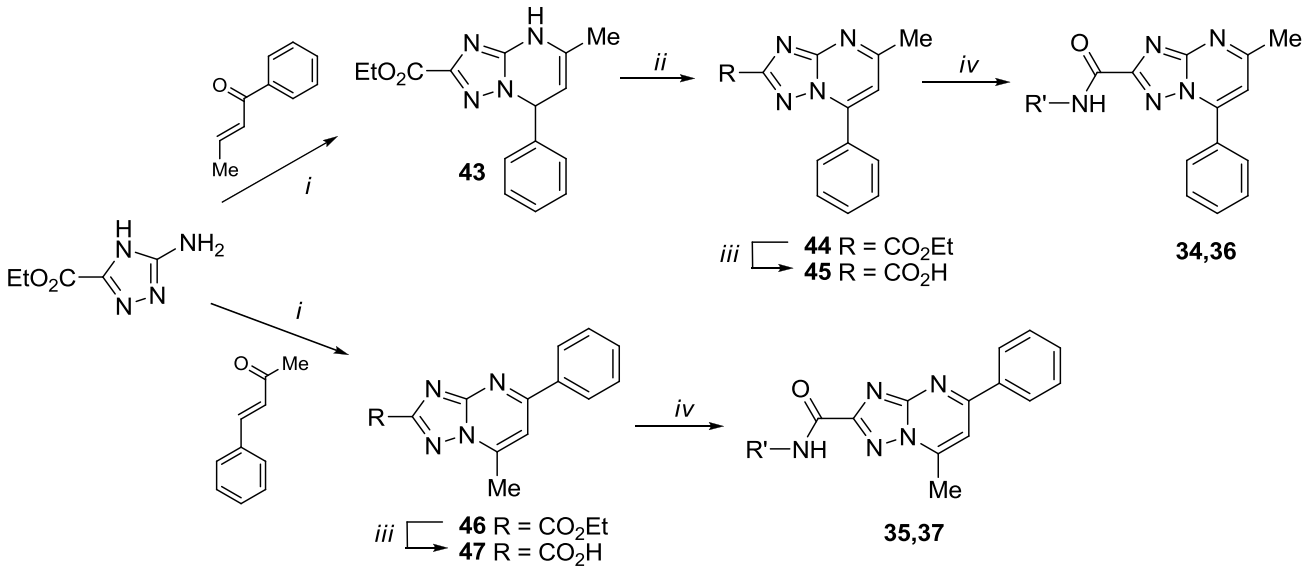

"Table of Contents Graphic"